Reply to anonymous Referee #1

Remo Dietlicher

November 1, 2018

Thank you for carefully reading our manuscript. We are happy for your expertise regarding satellite data. In the following we answer the individual points you raise:

Main comments: In the model evaluation section, the authors do not describe the dataset at all and do not explain why they chose these specific datasets to evaluate their model. For example, three datasets are used for the fluxes and no reason whatsoever is given to justify this choice. The authors must define/introduce the datasets, even briefly, and explain why they use these. Also, the observed interannual STD can be used as an uncertainty estimates when nothing else is available. In addition, their model evaluation is more of a qualitative comparison than a quantitative one although it is possible to quantify the bias more precisely (see specific comments for further details). It also looks like (it is not specified in the manuscript) they didnt make a consistent comparison between the CALIPSO-GOCCP cloud phase dataset and their model outputs, i.e., they didnt use the simulator for the cloud phase diagnostics, which make the results difficult to interpret. In the second part of the manuscript, I feel like reducing the number of categories in the final part of the study would help to better determine the origin of the ice bias. Id like the author to either do that or better explain why they chose these categories and what is the added value of making this choice. Finally, the authors could easily check at least one of the mechanism that supposedly lead to the overestimation of the ice cloud occurrences (the overlap assumption).
(Introduction): The goal of the paper is a little bit confused and not clearly stated. Also, it is not clear to me how 'As has been eluded to above, the formation history of a cloud plays a decisive role, both for mixed-phase and cirrus clouds'. The authors should state clearly than one expect biases to come either from ice behavior with respect to liquid within the mixed-phase temperature range or from ice formation at temperature below -38C, and better explain the reasons.
We have restructured the introduction to better motivate the study. We now highlight that the cloud phase partitioning is governed by the ice phase parametrizations and that we want to figure out which process dominates in our model.

Define the acronyms (e.g., CALIPSO, GOCCP, COSP, CERES etc...)
Done.

P2 L18-19: The sentence could be re-phrased, K14 found that even... among a some (or number, I believe they used 6) GCMs was not reduced.
Done. Actually when checking the exact models, it was interesting to see so many models from the CAM family.

P2 L6: I believe ice-containing clouds would be more appropriate. Why not to compare the snow water content + IWC between the REF and 2M models?
We diagnose the snow mass flux in REF, assuming that all snow will reach the ground within one model timestep. Therefore we can quantify the column-integrated amount of snow but there is no way to assign snow contents to individual levels.

P8 L8: but may indirectly affect the cloud in the tropics, especially considering the large amount of high clouds removed
This is true, we adjusted the text.

P8 L10 version night time? The authors do not explain what is a simulator at all and why using cosp here. The sentence does not tell much. The SQRT(X2) of the bias and the correlation pattern number would help better assess the improvement of the new model version.
We use day and night. We extended this paragraph to motivate the usage of COSP better. We now also compute the Pearson correlation coefficient and RMSE between the models and CALIPSO to allow for a more quantitative discussion.

Fig. 3: There is no height in Fig3 Adding the contour of the difference in the original cloud cover on the bottom plot (i.e., the contour of the blue color, $-5\,\%$ in bottom right plot of Fig. 2) could help identifying areas of improvement. It seems like there is no change at all in middle cloud, which are lacking even in areas with no overlying high-cloud which could cause shielding effect of the lidar.
The height axis must have disappeared by mistake, its in there again. Thank you for noticing this. Adding the $-5\,\%$ contour line to highlight areas where the new cloud cover parameterization acts is a good idea. The new scheme has been designed to make the transition from mixed-phase to cirrus clouds continuous and consistent with the parameterization of the formation of cirrus clouds. Improving the cirrus cloud structure is a nice side-product. Improving the mid-level cloud structure has not been the focus of this study.

P8 L18-22: Im not sure I understand the sentence: The fact... The authors state that changing microphysics does not affect CRE, that is not true (e.g., Cesana et al., 2017; their Fig. 3). The authors might get similar CREs because they tune the TOA fluxes. Also in their Fig. 4, it is clear that there are regional differences in the GCMs CREs, i.e., over the Southern Ocean. This bias is worsened by the new GCMs, probably because of less supercooled liquid sustained in the mixed-phase clouds. The authors do not explain why they chose these particular observation datasets. For the fluxes, I believe CERES-EBAF is the most relevant dataset for model evaluation also the longest period of time available (therefore a better climatological estimate of the present-day mean state), which is not defined either. Same thing for the cloud cover, no reason for these specific datasets and while it is mentioned that the simulator is used before (although it is not mentioned why) here no information is given whatsoever. I would recommend using only simulator-derived model outputs against GCM-oriented observation datasets, e.g., ISCCP, simulator Klein and Jakob, 1999 and dataset: Pincus et al., 2012, MODIS, simulator and dataset Pincus et al., 2012, cloudsat simulator Marchand et al., 2008 and dataset Marchand et al., 2010, CALIPSO, simulator Chepfer et al 2008; Dataset Chepfer et al., 2010. The interannual STD may be used as an uncertainty...
We have rewritten this paragraph to make clear that CRE is a consequence of tuning

TOA fluxes. The fact that it is more negative than what observations suggest hints at a structural problem in the model that is not specific to the microphysics scheme.
Regarding the TOA fluxes in Fig. 4, we agree that the original Figure was confusing. We now only use the CERES-EBAF dataset as suggested and plot the interannual STD as a measure of uncertainty. Furthermore, we compute the correlation and RMSE of the full 2D fields. We agree that these statistics provide interesting and important information for a more quantitative assessment of these fundamental model variables. This analysis revealed that the statement about the new model correlating better with the observations was false, even though the zonal mean suggested that.

P8L26: I would suggest adding In the new scheme (i.e., 2M, 4M)... to avoid confusion.
We replaced this sentence with something more precise.

P8L31: Again, it is not quantified at all, so hard to say. With these 2D quantities (i.e., cloud cover), it is easy to compute means, biases and correlation, so please do so and compare to CERES-EBAF.
This has been addressed in a previous comment.

It is striking to see how little change there is between 2M and REF in terms of cloud cover whereas the vertical cloud fractions are tremendously different. Did the authors look at the high-cloud cover as well? Can they give a hint of why such a small difference in the cloud covers? The cloud overlap may explain this.
The new and reference models differ most in high-level clouds and are fairly similar for mid- and low-level clouds. Since both models tend to underestimate the cloud fraction, the overestimation of the high-level cloud fraction in the reference model improves the total cloud cover in areas where the cloud fraction would be small otherwise. We agree that the reason for the smaller difference among the models in terms of total cloud cover as compared to the vertical structure is due to vertical overlap. This is now mentioned at the end of Section 3.2.

P9L5: Again very little information is given about the observational dataset and its weaknesses/strengths.
We extended this paragraph to motivate the use of the Li et al, 2012 dataset better.

P10 Sec. 3.6: Is the simulator used in that comparison or do the authors compare CALIPSO-GOCCP to the direct outputs of their models?
We do not use a simulator for Fig. 7 but added a new Fig. 8 including output from the COSP simulator. More details follow below.

P11 Sec. 4: While I agree that the method used here to determine the origin of the overestimation of cloud ice is good, it is not new and it has been used in the past for different topics and referred to as tendency (i.e., Brient et al., 2016). It is usually not possible to do so when comparing multiple models unless a specific experiment is designed to tackle a problem and requires these such as in Brient et al. (2016) -, which is why it does not often appear in multimodel studies.
We changed the text to highlight the reason why this diagnostic is very helpful to answer the specific question at hand 'where does ice come from?' and better differentiate this method from analyzing model tendencies. In a nutshell, tendencies are a snapshot of

the strength of processes but provide no history, which source-tagged tracers do. However, implementing our method requires additional prognostic tracers, a substantial effort, which makes it even more unlikely to be used in model inter-comparisons.

I do not understand what justify the use of so many types of clouds. The question is where does this ice come from? The answer is threefold from what I understand. Therefore, there should be three categories: Fraction of ice from heterogenous processes Fhet, from homogenous processes Fhom and from nucleation Fnuc. The total would be 100 % and figures would be easier to understand.
The goal of the cloud types defined in this study is to differentiate clouds with fundamentally different properties. A priori, we did not know what to expect but wanted to include all information that is available in the model. For example, we were interested to know whether mixed-phase clouds are so rare because (1) mixed-phase freezing occurs infrequently or (2) whether the subsequent ice growth is slow. Distinguishing ice and liquid dominated mixed-phase clouds allows quantifying both aspects: (1) mixed-phase freezing is only important in a small fraction of clouds and (2) the effect it has on the cloud phase partitioning is even smaller because a majority of mixed-phase clouds do not (or slowly) glaciate. Similarly, including the vertical cloud structure allowed to diagnose sedimentation in vertically adjacent cloudy layers as the relevant pathway for the transport of ice into the mixed-phase regime. A priori, it could also have been the case that e.g. sublimation in clear-sky levels is underestimated such that ice can pass too many subsaturated layers. Finally, we differentiate warm and cold liquid clouds to quantify the cloud amount that could be affected by freezing.
The sum of all cloud types is exactly the total cloud cover.

P13L15: But how to define unrealistic pathways when no observations are available to compare to?
We have rewritten this paragraph to be more precise about the use of our method and refrain from the word 'unrealistic' which we agree cannot be assessed by observations.

P14: Again, a fraction compare to the total would make more sense.
We assume this comment is regarding Fig 12 which is discussed on page 14. Having both plots at hand, we believe there is no benefit of normalizing by total cloud cover. Qualitative statements about the relative contribution to the total cloudiness can still easily be made.

P14L20: If the simulator is used, then the same weaknesses should affect the model outputs. Also, in the mixed-phase temperature regimes, the undef-phase category can be considered as mixed-phase likely. By using ice/total cloud frequency you are considering these undef-phase clouds as being liquid clouds, which is true in the tropics at warm temperature but unlikely at freezing temperatures. Once again, this section raises the question of whether the lidar simulator was used in Fig. 7.
Since we are not using a simulator for Fig. 7, we added a new Fig. 8 which compares the phase ratios versus temperature lines from the satellite, the model and the model + simulator. This was actually an interesting and worthwhile exercise. The overestimation at $T > 15\,°C$ is much reduced when using a simulator, implying that attenuation is very important in this temperature regime. It makes sense, since the thick cloud type is also optically thick, the lidar signal will always be attenuated in the lower part of these clouds.

Unfortunately, this implies that the satellite cannot be used to constrain the cloud phase partitioning in this temperature regime.
Figure 7 was inspired by Cesana et al. 2015 where they conduct a comprehensive model inter-comparison of phase ratio vs. temperature histograms (their Fig. 10). For the satellite panel we reproduced their Fig. 10 by using daily night-time data from here: ftp://ftp.climserv.ipsl.polytechnique.fr/cfmip/GOCCP_v3/3D_CloudFraction/grid_2x2xL40/2008/night/daily for the years 2008-2014. These files contain a variable called *cltemp_phase* which is computed as ice/(ice+liquid), i.e. neglects pixels where no phase can be assigned (undef). This corresponds exactly to the computation within the COSP simulator.

One could also look at particular latitude bands to avoid the influence of these thick clouds and see whether it impacts the Phase-T relationship, e.g., in the Arctic where these clouds are less frequent.
Thick and cirrus clouds are the dominant cloud type almost everywhere on the globe (see Fig. 11).

L13: Did the authors mean sedimentation of ice at warmer temperature? i.e., the mixed-phase temperature range?
We meant to say from colder (below $-35\,^{\circ}\mathrm{C}$) to warmer temperatures (i.e. the mixed-phase regime). This is now stated more clearly.

L15 Im not sure simplifying ice category from ice crystals and snow ice to only ice can be called as an improvement, Id rather use the word 'difference'.
It is an improvement in terms of the physical realism of the scheme at the cost of increased computational demand because sedimentation of ice crystals needs to be resolved. So improvement might indeed be a little bit too general and we replaced it with 'difference'.

L18-20: No cloud bias below $-35\,^{\circ}\mathrm{C}$ is shown in this paper and the biases are not well quantitatively quantified. I dont understand the expression 'arguably more reasonable tuning parameters'. This should be clarified.
We show that the reference model overestimates the cloud fraction at temperatures below $-35\,^{\circ}\mathrm{C}$ in Fig. 3. In the updated version of the manuscript we now compute the correlation and RMSE and are confident that the new cloud cover parametrization is not just a conceptual improvement but also leads to a more realistic cloud fraction for these high clouds. We removed the sentence about tuning parameters. Even though we are more happy with scaling process rates by a factor of 5 rather than 1000, they are fundamentally unconstrained so there is not really a metric to assess good and bad.

P16 L5-6: Checking this out by changing the sedimentation overlap to random (or even minimum) overlap and running a short 1yr or even a few month simulation should be relatively easy to do and would strengthen the conclusions.
Given all the changes above, the part that is referenced here has been removed.

Reply to anonymous Referee #2

Remo Dietlicher

November 1, 2018

Thank your for carefully reading our manuscript and the positive review. Below we elaborate on the points that you mention and outline how we addressed them.

I found it a bit confusing that the paper tries to do two very different things at once: (1) present validation of a new ice microphysics parameterization (that has already been described in a GMD article) against observations and (2) introduce new tracers to classify the origin of cloud ice, a technique that is applicable to new and old microphysics alike. Scientifically, the second part of the paper is far more interesting, and I feel the first part might have found a better home in the GMD paper. Perhaps there is a way to tie the two parts together a bit more in Sec. 5.2, by describing whether there are significant differences between the new and old microphysics, and in particular whether the new microphysics leads to an improvement. (I realize Fig. 7 does this for the state, but I dont see analogous discussion for the pathways.)
We completely agree that the validation part of this paper would have fit also together with the technical evaluation in the GMD paper. However, we chose this composition to segregate the idealized single column simulations which highlight the technical aspects of the new scheme from the global evaluation presented here.
Technically, one big improvement that the new microphysics scheme brings is a more readable and manageable code-base. This allowed to easily implement the formation pathway diagnostics. Porting this to the old microphysics code would have been a considerable effort which is why we cannot compare the pathway analysis between the models. The touching point is Fig. 7 where we see a similar phase ratio and thus assume that probably the same mechanisms are in place. Especially since we could trace the high frequency of ice clouds at high temperatures back to the vertical structure of clouds (thick category) which is a result of parametrizations that are similar or even identical in the two models. We briefly addressed this problem now in the introduction to Section 5.

I agree with the sentiment of the introductory paragraph of Sec. 4 (although I would make an exception for observations that permit inference of process rates or the relative importance of various processes). Of course, this paragraph comes right after a long section that does the exact thing the authors criticize. Perhaps this is an argument in favor of shortening Sec. 3 or moving parts of it to an appendix?
We don't see a viable way to evaluate GCM output other than comparing to climatologies derived from (satellite-)observations. Comprehensive case-studies which allow to infer microphysical process rates usually only target specific clouds and meteorological conditions which cannot easily be generalized to be used in a GCM. We therefore don't want do abandon spatio-temporally averaged model output but rather highlight the fact that in this kind of output a lot of valuable information is lost. In light of your comment, we

have rewritten this part of the introductory paragraph of Section 4 to be more precise.

The previous point notwithstanding, in Sec. 3 (Tab. 3 in particular), I was surprised that the authors provide an uncertainty range for radiative flux observations but not for the ice water path. IWP seems like the more directly relevant variable to evaluate the ice microphysics scheme. It would be nice to see whether passive microwave, MODIS, etc. IWP estimates are as far away from the model as CloudSat/Calipso. Also, why not add the TIWP in the REF model to Tab. 3 under the assumption that the sedimentation occurs within the time step? (And likewise for CIWP in the new configuration?)
You are right, it makes a lot of sense to include the uncertainty range for T/CIWP in Table 3. It has been added. We agree that IWP/C is the most relevant variable to evaluate the new (ice) microphysics scheme. Nevertheless, a direct comparison remains difficult due to uncertainties in the retrievals and the heterogeneous representation of ice in models. In our reference model ice is split up into in-cloud ice and stratiform and convective snow. The new model can uniformly describe stratiform precipitation but the uncertainty from convective ice still remains.
We do not think that we can use a 'diagnostic trick' to homogenize model output. The reference model diagnoses the snow mass flux as $P_{snow} = \int_0^{p_s} Sources - Sinks \, dp$ for the surface pressure p_s. The mass mixing ratio of snow therefore relies on the sedimentation velocity of snow which is rather uncertain since there is no prognostic information on the snow particle size. Similarly, computing CIWP for the new model would require a threshold size or fall velocity above which ice crystals are considered to be snow. This goes directly against a main benefit of the P3 scheme which is eliminating such threshold sizes.

In the discussion of deposition acting as a sink for cloud cover via the Sundqvist cloud cover scheme (Sec. 2.2), I would have welcomed a sentence or two on whether condensation analogously acts as a sink for cloud cover or how this is avoided. Also, the sentence 'However, this coupling also makes the sedimentation sink of cloud ice a sink for cloud fraction' made me wonder: isn't that realistic, desirable behavior?
For cloud water we do not have this problem as condensation/evaporation is given by Eq. (2) which is a form of saturation adjustment and does not allow supersaturation w.r.t. liquid water by definition. There is only a problem for cloud ice which either forms from a liquid cloud or nucleates directly from the vapor phase. Both pathways require substantial supersaturation w.r.t. ice. Therefore we need to specify what happens once the initial ice crystals have formed.
Regarding your second point we agree in principle. Our concern with this is mostly the increase of in-cloud ice crystal number concentrations and the resulting feedback loop involving the coupling of aggregation, sedimentation and cloud cover. This is discussed in Section 3.4 paragraph 3 where we argue that it explains the lower cloud cover found in the 2M as compared to LIM_ICE simulation.

Sec. 3.2, better agreement with GOCCP cloud cover: was this part of the tuning strategy, or did it emerge?
The main goal of the new cloud cover parametrization was to consistently extend the notion of the subgrid cloud fraction to the cirrus regime. In the reference model there is a mismatch between how the cloud fraction is diagnosed ($b = 1$ at ice saturation) and the cirrus cloud formation processes (efficient nucleation only at $RH =\sim 140\,\%$). Tying the

cloud cover and cirrus nucleation parametrizations together there is no freedom to tune the parametrization. We now highlight this in Section 3.2.

Sec. 4.3, last sentence: would 'cirrus-origin cloud' be less confusing terminology than cirrus?
This is a philosophical question that came up in the process of this project as well. In my eyes, a cirrus cloud does not lose its 'cirrus'-ness when it crosses a certain temperature threshold. I also like to be very cautious when using real-life intuition on model output. These readily sedimenting cirrus clouds seem to be much more prominent in the model-world than in real-life. So if anything, we could call it 'model cirrus' but then again I guess the 'model' part is implied.

Sec. 5.1, Fig. 10: The frequencies here are defined by volume. If they were defined by mass, which I assume would be equally valid but give greater weight to warmer clouds, would the conclusions be very different?
They are actually defined by air mass, not volume. We refrained from calling it cloud mass as this could be confused with the mass of cloud condensate which would drastically alter the relative contributions. We do not believe that there is a substantial change if we use air volume or mass. If we were to use volume the relative contribution of cirrus would probably be somewhat higher.

Sec. 5.2, l. 19-21: This seems out of place here; maybe a better place would be in Sec. 3.6?
You are right in that this would fit nicely in Section 3.6 when Fig. 7 is discussed. However, we need to introduce the formation pathways (Section 4) before we can discuss the different origins of cloud ice. We extended the introductory paragraph to Section 5 to better tie the two parts together.

p. 1, l. 15: 'radiative forcing' → 'radiative effect', since the clouds are part of the climate system?
You are right!

p. 2, l. 21: I kept wondering for the rest of the manuscript why the homogeneous freezing threshold is −35 °C rather than −38 °C.
In theory the threshold is close to −38 °C. However, our model traditionally used −35 °C (based on Lohmann and Roeckner, 1996) as a freezing threshold which is why we use this when talking about the model. However, this number does no longer appear in any of the parametrizations of the new model since homogeneous freezing and cloud cover parametrizations have been replaced from the reference model (where a threshold value of −35 °C is used).

p. 3, l. 24: Can you comment on how applicable this is to other models?
Since it requires solving additional prognostic tracers according to Eqs. (5), (6) and (A1), it is probably unrealistic to implement in a large model intercomparison. However, these tracers are easily implemented if the cloud tendencies are accessible in the code (S-terms in the equations). This is why it is hard to do for our reference model where the computation of tendencies is often intertwined with local variable updates.

Fig. 2: Only color scale for differences is included in the plot.
This is not the case in my PDF-viewer.. Something to double-check when type-setting.

Thank you for finding various typos, they have all been corrected.

The ice formation pathways in the aerosol-climate model ECHAM-HAM

Remo Dietlicher[1], David Neubauer[1], and Ulrike Lohmann[1]

[1]Institute for Atmospheric and Climate Science, ETH Zürich, Universitätstrasse 16, 8092 Zürich, Switzerland.

Correspondence to: Remo Dietlicher (remo.dietlicher@env.ethz.ch)

Abstract. Cloud microphysics schemes in global climate models have long suffered from a lack of reliable satellite observations of cloud ice. At the same time there is a broad consensus that the correct simulation of cloud phase is imperative for a reliable assessment of Earth's climate sensitivity. ~~Combining new satellite products (from CloudSat and CALIPSO) and physically-based ice microphysics parameterizations allows for rapid progress in reducing~~ At the core of this problem is understanding of the causes for the inter-model spread ~~in predicting the~~ of the predicted cloud phase partitioning~~at sub-zero temperatures~~. This work introduces a new method to build a sound cause-and-effect relation between the microphysical parameterizations employed in our model and the resulting cloud field through a quantitative ~~cloud~~ ice formation pathway analysis. We find that ~~heterogeneous freezing in super-cooled~~ freezing processes in supercooled liquid clouds only ~~dominates~~ dominate ice formation in roughly $5\,\%$ of the simulated ~~cloud volume~~clouds, a small fraction compared to ~~almost of the cloud volume governed by homogeneous freezing~~ roughly $64\,\%$ of the clouds governed by freezing in the cirrus temperature regime below $-35\,°\mathrm{C}$. ~~Compared to the CALIPSO-GOCCP satellite product, our model overestimates the relative frequency of occurrence of cloud ice in the~~ This pathway analysis further reveals that even in the mixed-phase ~~temperature~~ temperature regime between $-35\,°\mathrm{C}$ and $0\,°\mathrm{C}$, the dominant source of ice is the sedimentation of ice crystals that originated in the cirrus regime. The ~~ice formation pathway analysis reveals that this is caused by too much cloud ice propagating from the cirrus into the mixed-phase cloud regime, an unexpected result. This suggests that further efforts to improve the cloud phase partitioning must target cloud overlap assumptions for sedimentation and the related below-cloud sublimation~~simulated cloud phase partitioning compares well with the CALIPSO-GOCCP satellite product. However, a large fraction of simulated ice clouds is in the blind spot of the lidar, in the lower part of optically thick clouds.

1 Introduction

Clouds are an important modulator for Earth's climate. They ~~excert~~ exert a net radiative ~~forcing~~ effect of approximately $-20\,\mathrm{W\,m^{-2}}$ and thus significantly cool the planet (Boucher et al., 2013). Compared to this, the forcing induced by well-mixed greenhouse gases since pre-industrial times is almost one order of magnitude smaller, approximately $3\,\mathrm{W\,m^{-2}}$ (Myhre et al., 2013), and has the opposite sign associated with a warming. Small changes in the cloud radiative ~~forcing~~ effect can therefore easily offset or strengthen a greenhouse gas induced warming. In fact, there is a broad consensus that clouds contribute the

largest uncertainty for climate projections in state-of-the-art atmospheric general circulation and Earth system models (Flato et al., 2013).

The models that contributed to the Community Model Intercomparison Project Phase 5 (CMIP5) generally agree that cloud adjustments to a warming climate will likely further reinforce the initial warming, a positive feedback loop. Clouds are expected to become fewer, higher and optically thicker in the global mean (Zelinka et al., 2013).

The warming response of cloud ice has been hypothesized to counteract and therefore reduce the global mean, net positive cloud feedback through a transition from optically thin ice clouds in the present day climate to optically thick liquid clouds in a warmer climate (Mitchell et al., 1989; Storelvmo et al., 2015; Ceppi et al., 2016; Frey and Kay, 2018). The magnitude of this so-called cloud phase feedback strongly depends on the simulation of the present-day cloud phase partitioning in models. It is well established that models tend to underestimate the ratio of supercooled liquid water to ice in present-day conditions (Cesana et al., 2015). This leads to an overestimation of the magnitude of the cloud phase feedback (Li and Le Treut, 1992; Terai et al., 2016; Tan et al., 2016) in a greenhouse gas induced, warmer climate in some models. Recent modeling efforts challenge the universality of this finding (Lohmann and Neubauer, 2018; Bodas-Salcedo, 2018), calling for a more comprehensive description of ice formation pathways in GCMs.

Especially sensitive to global warming is ice in mixed-phase clouds, predominantly originating from heterogeneous immersion or contact freezing of mineral dust (Atkinson et al., 2013; DeMott et al., 2015; Kanji et al., 2017). Those clouds are usually found in the temperature range between $-38\,^{\circ}\mathrm{C}$ and $0\,^{\circ}\mathrm{C}$ which we therefore refer to as the mixed-phase temperature regime. Beyond the theoretical and experimental uncertainties of the freezing mechanisms (Welti et al., 2014; Ickes et al., 2015; Marcolli, 2017), a realistic representation of cloud glaciation is further complicated by uncertainties in the parameterization of subsequent ice growth and sedimentation. Due to the lower saturation water vapor pressure over an ice crystal compared to a liquid droplet surface, cloud ice can grow below water saturation, eventually leading to evaporation of the cloud droplets. This process is called the Wegener-Bergeron-Findeisen (WBF) process and can glaciate a cloud within minutes to hours (Korolev and Isaac, 2003), depending on the number of ice crystals, temperature and vertical velocity of the air parcel.

Due to the complex processes governing mixed-phase clouds, models inhibit a very large spread in the simulation of the phase partitioning (Fan et al., 2011; McCoy et al., 2016). A model intercomparison study of Komurcu et al. (2014) found for the ~~models~~ 6 models (ECHAM6, CAM-IMPACT, CAM-Oslo, CAM5.1 MAM3, CAM5.1 MAM7, SPRINTARS) in their study that even for the same ice nucleation parameterizations, the spread in the simulated phase partitioning among the models was not reduced.

A significant portion of cloud ice is found at temperatures below $-38\,^{\circ}\mathrm{C}$. There, ice crystals can freeze homogeneously from pre-activated cloud droplets (Lohmann et al., 2016) and deliquesced aerosols (Koop et al., 2000) or nucleate directly on an ice nucleating particle (INP). The latter two processes do not require water saturation, leading to fundamentally different types of cirrus clouds (Krämer et al., 2016; Wernli et al., 2016; Gasparini et al., 2018) with significant differences in the respective microphysical and thus optical properties, highlighting the need for a correct representation of ice formation pathways of all clouds containing ice, not just those in the mixed-phase regime.

~~In this study we employ~~ These complex, sub-grid scale processes can only be studies through idealized laboratory measurements and inferred from comprehensive field studies which are usually conducted over small areas. Being weakly constrained, ice process parameterizations differ greatly among models and with that different ice formation pathways can be favored leading to the wide spread in phase partitioning among models (Cesana et al., 2015; McCoy et al., 2016). To find the parameterizations that control the cloud phase partitioning, we need to quantify the impact each process has on the simulated cloud fields.

The amount of ice that forms following a nucleation event in either a mixed-phase or cirrus cloud strongly depends on the available humidity and, in the case of mixed-phase clouds, liquid water. A strong nucleation event does not necessarily induce a long-lived or massive ice cloud and vice versa. Furthermore, sedimentation of cloud ice disconnects ice initiation and growth regions which further complicates diagnosing the causal link between the parameterized microphysical processes and the observed cloud state. Traditional, spatio-temporally averaged model output usually reports the mean state of the cloud fields and sometimes microphysical tendencies, but does not allow to trace back the dominant microphysical formation mechanisms due to the reasons above. Unlike the real atmosphere, which does not directly reveal its governing processes, the models do so by definition. Here we harvest this additional information that is present in the models by introducing additional tracers to quantify the microphysical ice formation pathways along with the model integration to assess the importance of different ice initiation and growth mechanisms.

Furthermore, we use the pathway analysis to classify clouds and accumulate statistics on their properties. The benefit of cloud classification is well established and has a long history. A common method is the identification of dynamical cloud regimes to compute conditional statistics (Jakob and Tselioudis, 2003; Williams and Tselioudis, 2007; Williams and Webb, 2009; Tsushima et al., 20
These methods use high-frequency output and short-term temporal aggregation of cloud top temperature vs. cloud optical thickness histograms together with clustering algorithms, classifying the mean dynamic states over the aggregation period. Our method focuses on the microphysics of cloud formation linking parameterizations and the resulting cloud fields. This link is essential to identify the parametrizations responsible for potential model to model or model to observation mismatches.

This study is based on an adapted version of the Predicted Bulk Particle Properties (P3) scheme of Morrison and Milbrandt (2015) for the use in a GCM. Single category ice phase microphysics schemes have recently also been implemented in the Community Atmosphere Model Version 5 (CAM5) GCM (Eidhammer et al., 2017; Xi et al., 2017). Dietlicher et al. (2018) (hereafter D18) provides a detailed description of the technical aspects of the implementation of P3 in ECHAM6-HAM2, the GCM we use in this study. This scheme has the decisive advantage of representing cloud ice in a consistent manner, predicting the particle size distribution as well as the mass-to-size relationship. It employs one single, prognostic ice phase category, rendering heuristic conversion rates between in-cloud and precipitation type ice hydrometeors unnecessary. Process rates are computed offline and read back from look-up tables. This allows to integrate each process rate over the entire particle spectrum. For example, our scheme consistently represents the size dependence of the depositional growth rate using a size-dependent ice crystal capacitance. Simplified, size-independent ice crystal growth rates are hypothesized to significantly contribute to the large spread among models in the simulated phase partitioning (Fan et al., 2011).

As has been eluded to above, the formation history of a cloud plays a decisive role, both for mixed-phase and cirrus clouds. Traditional model output is heavily aggregated spatially and temporally. Therefore, information on the cloud formation pathways is lost and must be inferred retroactively from the aggregated model states. Cause-and-effect relations between the microphysical parameterizations and the resulting cloud state are blurred as a result, which is a problem for model development where such relations are essential to target faulty or unrealistic parameterizations. Unlike the real atmosphere which does not directly reveal its governing processes, the models do by definition. This retroactive inference is therefore unnecessary and in part defeats the purpose of model simulations: the forward integration of differential equations. Here we introduce a new method to trace and quantify the microphysical cloud formation pathways and use cloud classification to compute cloud type statistics.

The benefit of cloud classification is well established and has a long history. A common method is the identification of dynamical cloud regimes to compute conditional statistics (Jakob and Tselioudis, 2003; Williams and Tselioudis, 2007; Williams and Webb These methods use high-frequency output and short-term temporal aggregation of cloud top temperature vs. cloud optical thickness histograms together with clustering algorithms, classifying the mean dynamic states over the aggregation period. Our method focuses on the microphysics of cloud formation linking parameterizations and the resulting cloud field. This link is essential to understand the simulated cloud field and can be used as an effective tool to identify deficient parameterizations.

This studyis composed of two partsThis study can be divided into two parts. First, we show how the new model performs on the global scale and then introduce the method to elucidate the ice formation pathways in the second part of this study. In Sect. 2 we highlight the main differences in the model employed here our model compared to the reference model version ECHAM6.3-HAM2.3 and discuss the new cloud fraction parameterization that has been added since the previous description of the new model version in D18. We validate evaluate the simulation of clouds, with a special focus on cloud ice, against a series of satellite observations in Sect. 3. In the second part, we introduce additional prognostic equations that are solved to quantify cloud ice formation pathways in Sect. 4which are used to . In Sect. 5 we compile a climatology of cloud types in Sect. 5 to define explicit targets for further progress in microphysical parameterizationsbased on these ice formation pathways and demonstrate how they can help understand cloud phase partitioning.

2 Model description

The improvements to the previous model version ECHAM6.3-HAM2.3 (Neubauer et al., 2014)) (hereafter called the reference model) are twofold. In the new model, cloud ice is a fully prognostic quantity, i.e. the advection equation for vertical transport (sedimentation) is solved online. Describing all ice particles with only a single category based on Morrison and Milbrandt (2015) no longer requires the heuristic partitioning between in-cloud ice and precipitating snow. The technical details of the model regarding prognostic treatment of sedimentation and the associated numerical stability restrictions on the time-step as well as an inter-comparison of the different ice representation schemes can be found in D18. Here we will focus on the global evaluation of the new model both in terms of feasibility of the results as well as computational performance.

The predicted bulk particle properties scheme (P3) presented in Morrison and Milbrandt (2015) predicts 4 properties of the ice particle distribution: the total ice mass mixing ratio q_i, the total ice number mixing ratio N_i, the rimed ice mass mixing ratio q_{rim} and the rimed ice density b_{rim}. Originally developed for the Weather Research and Forecasting model (WRF), the scheme was not intended for the coarse resolution of GCMs and climate projections. As we have shown in D18 by idealized single column model (SCM) simulations, GCMs are likely unable to properly represent small-scale weather features like squall lines to produce significant rimed ice formation. We test this hypothesis in the global setup of ECHAM-HAM in this paper.

The single conceptual deviation from the microphysics scheme described in D18 concerns the sub-grid cloud cover parameterization. While this work focuses on the importance of the representation of cloud ice, the sub-grid cloudiness is a fundamental property of clouds in GCMs, governing both cloud-radiation and cloud-precipitation interactions.

The approach taken in D18 tried to minimize the difference between the new and the reference model by extending the approach of Sundqvist et al. (1989) (hereafter S89) to ice clouds with a smooth transition from liquid water to ice clouds. As we will discuss in Sect. 3, this scheme leads to a strong positive bias of cloud cover for cirrus clouds. Therefore, we used a slightly different cloud cover scheme here.

The cloud cover scheme has also implications for the growth by condensation and deposition. Diagnosing sub-grid cloud cover from the large-scale relative humidity creates a tight link between the cloud fraction and growth by condensation or deposition. The fundamental concept of the S89 scheme is that convergence of humidity within a grid-box contributes to an increase in total cloud water by condensation and deposition as well as an increase of the cloud fraction through moistening of the grid-box. Here we extend this idea to cold clouds and implement a cloud cover scheme which treats the microphysical structure of ice clouds consistently, requiring mixed-phase clouds to form via the liquid phase and allowing supersaturation in the cirrus regime.

2.1 Sub-grid cloud fraction

The original sub-grid cloud cover scheme of S89 does not consider cloud ice and assumes that a grid-box will be fully covered by the cloud if the water vapor mixing ratio q_v surpasses the liquid water saturation mixing ratio q_{sw}, i.e. the relative humidity with respect to liquid water s_w satisfies $s_w = q_v/q_{sw} = 1$. Cloud cover b increases with increasing s_w as:

$$b = 1 - \left(\frac{s_{max} - s_w}{s_{max} - s_{min}} \right)^{\frac{1}{2}}. \tag{1}$$

The parameter s_{min} is the threshold relative humidity for sub-grid cloudiness below grid-box mean water saturation and $s_{max} = 1$. The assumptions underlying Eq. (1) are reasonable for synoptic-scale warm clouds. However, this scheme cannot be easily extended to cold clouds where a grid-box may or may not contain cloud ice in the mixed-phase regime, rendering the global use of s_w for all temperatures inadequate. At the same time, relative humidity with respect to ice (s_i) can reach values higher than $140\,\%$ before ice nucleates from deliquesced aerosols (Koop et al., 2000), which is inconsistent with the use of $s_{max} = 1$ for ice clouds at cold temperatures. A few approaches exist to overcome either of these aspects. In the following we present the reasoning that ~~lead~~ led to the development of the new method used here. For an overview, see Fig. 1.

As illustrated in the top panel of Fig. 1, Lohmann and Roeckner (1996) (the method used in the reference model) replaced s_w in Eq. (1) by s_i if a threshold amount of ice is exceeded within the grid-box. This approach has the draw-back that clouds artificially expand upon glaciation because of the lower saturation water vapor pressure over ice than over liquid water. A similar approach is taken in Morrison and Gettelman (2008) (and D18; illustrated by the middle panel in Fig. 1) where instead of the discontinuous transition from liquid water to ice saturation, the saturation liquid and ice water vapor mixing ratios are interpolated between q_{sw} and q_{si} as a function of temperature in the mixed-phase regime. The draw-back here is, that this interpolated value is not directly relatable to a physical quantity as it does not arise from a valid solution of the Clausius-Clapeyron equation. Both of these schemes are not designed to allow for sub-grid clouds in the cirrus regime where s_i needs to be well above 1 for ice nucleation to occur, i.e. all cirrus clouds formed by homogeneous freezing will occupy the entire grid-box. Supersaturation with respect to cloud ice has been accounted for in the cloud cover scheme by Gettelman et al. (2010) where individual cloud fractions for liquid water and ice clouds are computed with a functional dependency of the cloud fraction $b(s)$ similar to Eq. (1) but relaxing the relative humidity for complete cloud coverage to $s_{max} = 1.1$ for ice clouds and treating the value of s_{max} as a model parameter.

The cloud fraction parameterization used in our microphysics scheme is very similar to this last approach, but we do not separate cloud cover for liquid and ice clouds. After all, in the mixed-phase regime we expect ice clouds to originate from liquid clouds ~~(Hande and Hoose, 2017)~~(Ansmann et al., 2009; Hoose et al., 2010; Hande and Hoose, 2017). Furthermore, the magnitude of ~~super-saturation~~ supersaturation for complete cloud cover ~~is rather~~ in Gettelman et al. (2010) is arbitrary. The scheme presented here uses a limit which is consistent with the parameterization of ice nucleation based on the theory of Koop et al. (2000). This scheme is illustrated in the bottom panel of Fig. 1.

One can associate s_{min} and s_{max} in Eq. (1) with the minimal relative humidity below which clouds start to evaporate and the maximal relative humidity which can be reached before the cloud covers the entire grid box. These two constraints provide some guidelines on how to extend the S89 scheme to cold clouds.

For clouds that form via liquid water, we assume that s_{max} is reached at liquid water saturation, e.g. when liquid water is assumed to condense immediately, which is a reasonable assumption for stratiform clouds. At temperatures warmer than $-35\,^{\circ}\mathrm{C}$, any ice must form via liquid water, consistent with the above mentioned lidar observations and modeling studies~~(Ansmann et al., 2009; Hoose et al., 2010)~~. For colder temperatures, it has been shown (Koop et al., 2000) that ice can nucleate from deliquesced aerosols already below liquid water saturation.

The minimal relative humidity s_{min} must be chosen such that ice does not sublimate above ice saturation. Cloud ice can sediment into and form within the mixed-phase regime. For this reason, and in order to retain sub-grid cloudiness for warm clouds, $s_{min} \leq 1$ must hold for all temperatures.

2.2 Growth by condensation and deposition

The water vapor available for condensation is linked to the cloud cover b by:

$$Q = -b(\Delta q_v - \Delta q_{sw}) \tag{2}$$

where Δq_v is the moisture convergence in the grid-box by the resolved transport and Δq_{sw} is the change in liquid water saturation water vapor mixing ratio according to the Clausius-Clapeyron equation. Growth by deposition A is computed as a function of the relative humidity with respect to ice s_i (see e.g. D18):

$$A = \Delta t N_i \alpha_m f_v \frac{4\pi C(s_i - 1)}{F_k^i + F_d^i} \tag{3}$$

where $\alpha_m = 0.5$ is the probability of a water vapor molecule to successfully be incorporated into an ice crystal, Δt is the model time step and C is the mean ice particle capacitance integrated over the particle size distribution. The parameters F_k^i and F_d^i are thermodynamic parameters depending only on temperature.

The maximal amount of water that can deposit in a single time step is ~~is~~ given by:

$$Q_i = Q + q_l + (q_v - q_{si}) \tag{4}$$

where q_l is the liquid water mixing ratio and q_{si} is the saturation water vapor mixing ratio with respect to ice. Equation (4) implicitly represents the WBF process in mixed-phase clouds through the inclusion of q_l. The last term in Eq. (4) allows any water vapor which is supersaturated with respect to cloud ice to deposit onto ice crystals and thus requires to add q_i to the water vapor mixing ratio for the computation of the relative humidity in Eq. (1) to prevent clouds from shrinking due to deposition. To account for ice clouds, we replace the relative humidity with respect to liquid water s_w in Eq. (1) by ~~a~~ the more general relative humidity term s ~~which is~~ defined below.

Combining the considerations for growth by condensation/deposition and the computation of cloud fraction, we obtain the key parameters for the computation of sub-grid cloudiness in Table 1. Two new parameters are introduced: the critical relative humidity with respect to liquid water for warm clouds K, which is equivalent to the parameterization for warm clouds used in the reference model and based on Xu and Krueger (1991), and the relative humidity required for nucleation of ice from deliquesced aerosols s_{koop} according to the activation theory of Koop et al. (2000) in the cirrus regime.

Two versions of the s and Q_i terms are given in Table 1 and represent two different methods to treat depositional growth in the mixed-phase regime. They bracket the main problem associated with cloud ice when diagnosing cloud cover from relative humidity. Cloud ice should be able to grow as long as water vapor is supersaturated with respect to ice. Since we are using the relative humidity with respect to liquid water (which is lower than the relative humidity with respect to ice) as maximal relative humidity s_{max} in the mixed-phase regime, ice growth below water saturation leads to a decrease in relative humidity and therefore lowers the cloud fraction b. Therefore we implement two versions of the new scheme. The first, default, method (subscripts 1) links cloud cover to the ice mass mixing ratio. It allows cloud ice to grow below liquid water saturation and adds cloud ice to water vapor for the computation of s in Eq. (1) to avoid cloud shrinking by vapor deposition. However, this coupling makes the sedimentation sink of cloud ice also a sink for cloud fraction. We test the sensitivity of this coupling with a second method (subscripts 2) where ice growth is inhibited below water saturation in the mixed-phase regime.

3 Model ~~validation~~evaluation

We evaluate the new model against a series of satellite observations as well as the reference model and test sensitivities to parameterization choices. Namely, we extend the investigation of ice properties presented in D18 to the global setup of ECHAM-HAM and assess the behaviour of the new cloud cover parameterization. Furthermore, we use an updated version of the cirrus parameterization, including heterogeneous ice nucleation of mineral dust at temperatures below $-35\,^{\circ}\mathrm{C}$ at low ice supersaturation based on Kärcher et al. (2006) (implementation courtesy of Steffen Münch, personal communication).

Results from 5 different model configurations for 10 years from 2003 to 2012 are shown, one with the reference model (ECHAM6.3-HAM2.3; REF) and 4 with the new scheme. We assess the influence of rime properties in the full P3 scheme (4M) by comparison with a model configuration where the rime properties are set to zero ($q_{rim} = b_{rim} = 0$) (2M). For the reasons presented below, we use the latter as the default configuration of the new model. With 2M as the starting configuration, we then investigate the effect of the artificial sedimentation-cloud cover feedback introduced by the new cloud cover scheme by limiting ice growth to liquid water saturation (LIM_ICE) and use an updated version of the cirrus cloud parameterization which includes heterogeneous ice nucleation on mineral dust below $-35\,^{\circ}\mathrm{C}$ (HET_CIR). The simulations and the employed tuning parameters are summarized in Table 2. The tuning parameters have been adjusted ~~to meet the TOA energy flux constraints~~ such that the model is in radiative balance at TOA for the simulations 2M, HET_CIR and REF.

3.1 Computational performance

The new model employs an adaptive time-stepping scheme to achieve numerical stability for the solution of the vertical advection equation for prognostic sedimentation of cloud ice. Sub-stepping the microphysics scheme comes at a cost, quantified by the CPU time column in Table 2. The numbers shown are computed from one year of simulation. Numbers vary by a few percent between runs, illustrated by the differences between the 2M, LIM_ICE and HET_CIR simulations which are comparable in terms of model complexity. Compared to the reference model, the new model runs approximately $25\,\%$ slower in the 2M/LIM_ICE/HET_CIR setups and $40\,\%$ slower in the 4M setup. This difference is mainly due to the high fall-speeds of rimed particles in the 4M simulation, which require more sub-steps. Compared to this, the cost of advecting two additional tracers is small.

3.2 Comparison to the reference model

Two main differences between the new model and the reference model are immediately evident from Table 2. The single category ~~does no longer require~~ no longer requires heuristic parameterizations for falling ice crystals and snow formation. At the same time, the new cloud cover parameterization allows to reduce the scaling factors, effectively bringing the parameterizations closer to their conceptual origin.

To illustrate the most prominent differences in the simulated cloud field, we compare cloud water contents (ice and liquid) as well as cloud cover in Fig. 2 of the new model in the 2M configuration to the reference model. For these quantities, the differences between the different configurations of the new model are small. It is evident ~~,~~that the new model produces a lot

more ice than the reference model. A large part of the difference can be explained by the fact that the single category scheme includes cloud ice and snow while snow is a diagnostic quantity which is not included in the ice water content in the two-category scheme employed in the reference model. Of course there are other contributing factors like parameter tuning and the cloud cover parameterization which are hard to disentangle.

In the simulated cloud liquid water there is no significant structural difference; the 2M simulation has slightly higher values everywhere. As the warm phase is not directly affected by the changes in cloud ice and the cloud cover parameterization, the differences are due to different autoconversion tuning parameters (γ_r in Table 2) and interactions with the ~~ice phase~~new cloud cover and ice phase parametrizations.

The cloud cover differs significantly due to the new cloud cover parameterization in the new model. Differences are most pronounced in the cirrus regime where a cloud now only covers the entire grid-box at the high supersaturation needed for homogeneous nucleation of solution droplets ~~.~~(see Sect. 2). Since this leads to a substantial difference in the cirrus cloud cover, we compare the reference model and the 2M configuration of the new model to satellite data in the following. For this purpose, we make us of the Cloud Feedback Model Intercomparison Project (CFMIP) Observation Simulator Package (COSP) (Bodas-Salcedo et al., 2011), which has already been implemented in ECHAM6-HAM2, and compare its output to the appropriate satellite product; the Cloud-Aerosol Lidar and Infrared Pathfinder Satellite Observation (CALIPSO), i.e. the GCM oriented CALIPSO cloud product (GOCCP) (Cesana and Chepfer, 2013). Using a simulator allows for a consistent comparison of model output and satellite derived cloud fields by minimizing artificial biases introduced by different cloud diagnostics and accounts for instrument sensitivity, which is particularly important for CALIPSO to account for the attenuation of the lidar signal.

The comparison to the cloud cover climatology from 2006 to 2012 of the CALIPSO-GOCCP product ~~(Cesana and Chepfer, 2013)~~ in Fig. 3 reveals that the new scheme fits better to ~~observations~~the observed cloud structure (Pearson correlation coefficient of 0.79 in the new model versus 0.70 of the reference model), despite an overall ~~low bias. For this comparison we used the COSP simulator (Bodas-Salcedo et al., 2011).~~ underestimation of cloudiness. It is worth noting that this underestimation is a consequence of the new cloud cover parametrization and not a result of model tuning. The distinct jump in cloud fraction anomalies in the reference simulation is a consequence of the discontinuous description of cloud cover from the mixed-phase temperature regime (0 °C to −35 °C) to the cirrus regime (colder than −35 °C) that has been removed by the new scheme. Despite this improvement in terms of the vertical cloud structure, we find that the total cloud cover is worse in the new model. The bottom left panel in Fig. 4 shows that the total cloud cover is differs less between the two models than their difference in high cloud cover. This is probably due to the vertical overlap of high-level clouds with mid- and low-level clouds that already cover the entire grid-box. In areas where there are no mid- and low-level clouds, the large amount of high-level clouds in the reference model can partly offset the overall underestimation of the total cloud cover. As a result, the reference model performs better in terms of RMSE for this variable.

3.3 Model tuning strategy

Model tuning has been conducted for the reference model (REF) and the two configurations of the new model 2M and HET_CIR while the 4M and LIM_ICE configurations use the same tuning as 2M. A summary of global, annual mean quantities is shown in Table 3. The main target of the tuning process has been the global, annual mean shortwave (SW) and longwave (LW) fluxes at TOA as well as the sum of the two. With the tuning parameters summarized in Table 2 we have a direct handle on the ~~net~~ global, annual mean cloud radiative effect (CRE) at TOA, defined as the difference of all-sky and clear-sky radiative fluxes. To reach our SW and LW radiation ~~targets~~ as well as the radiation imbalance tuning targets at TOA, we adjust the CRE. ~~The fact that all the~~ A consequence of this tuning strategy is that all model simulations (including the reference model with ~~an~~ a substantially different microphysics scheme) ~~find a~~ have a net CRE of roughly $-26\,\mathrm{W\,m^{-2}}$ ~~,~~ (depending on the achieved imbalance) which is more negative than any of the observational estimates ~~, highlights that CRE is merely a result of tuning TOA radiative fluxes and~~ and points at a structural problem in the model which is not specific to the ~~cloud~~ microphysics scheme. ~~The same is true for the hydrological cycle. Precipitation~~

We compare the simulated zonal, annual mean precipitation to the Global Precipitation Climatology Product (GPCP) (Adler et al., 2018) for the years 2003 to 2012. Total precipitation is largely governed by the rate of evaporation at the surface. As the sea surface temperature is prescribed ~~an~~ and most evaporation occurs over the oceans, cloud microphysics and convection parameterizations must produce similar amounts of total surface precipitation.

The lower cloud cover of the 2M and 4M simulations as compared to the LIM_ICE simulation is a direct consequence of the coupling of cloud ice and cloud cover. There are two main contributors: 1) ~~In the new scheme, the~~ The LIM_ICE configuration does not link the sedimentation sink of cloud ice ~~is also a sink for cloud cover and~~ to cloud cover while the other configurations (2M, 4M and HET_CIR) do and 2) ~~in~~ the LIM_ICE configuration limits depositional growth of ice crystals ~~is limited~~ and therefore the removal of water vapor by ice sedimentation is weaker, leaving more humidity in the atmosphere which in turn leads to more clouds.

~~The 2M, 4M and HET_CIR configurations of the new model all allow for a more realistic zonal distribution of the LW CRE than the reference model , despite an overall low bias (Fig. 4).~~ For the TOA energy fluxes we use the climatology from 2000 to 2017 from the Clouds and the Earth's Radiant Energy System (CERES) Edition-4.0 Energy Balanced And Filled (EBAF) (Loeb et al., 2018) product for the model evaluation.

Without the overestimation of cirrus cloud cover, we can reduce the convective rain formation rate γ_{cpr} to values closer to the pure ECHAM6 (without online aerosols from the HAM model and a single moment cloud microphysics scheme, see Stevens et al. (2013)) model with a value of $2 \times 10^{-4}\,\mathrm{s^{-1}}$ (Mauritsen et al., 2012). This allows to retain more water vapor in the updraft cores, thus enhancing the formation of tropical cirrus clouds in the outflow regions of convective anvils, associated with a ~~strong LW CRE .~~ more pronounced peak in the LW CRE in the tropics (Fig. 4). However, we only find a slightly better correlation with the CERES EBAF dataset than the reference model for the 2M, 4M and HET_CIR configurations while the LIM_ICE configuration correlates slightly worse. The root mean square error is worse in all configurations of the new model than in the reference model. This is most likely a consequence of the different tuning in the two models. In the reference model

both LW and SW CRE are stronger while the TOA fluxes are at the lower end of the tuning target in terms of magnitude, cf. Table 3.

3.4 Cloud ice

~~We~~ In Fig. 5 we evaluate the representation of cloud ice in the new model against the ~~data set~~ dataset compiled from CloudSat and CALIPSO retrievals by Li et al. (2012)~~which include observations of cloud ice (CIWC) and total ice content (TIWC; including snow and ice in short-lived, convective anvils~~. This dataset is based on three different cloud water content products: 2B-CWC-RO4 (Austin et al., 2009), DARDAR (raDAR/liDAR) (Hogan, 2006; Delanoë and Hogan, 2008, 2010) and 2C-ICE (Deng et al., 2013). This dataset has the advantage that considerable effort has been put into the distinction between in-cloud ice in stratiform clouds (CIWC) and snow from stratiform clouds and convective cores (TIWC). The ~~comparison is given in Fig. 5. With a single category , the cloud ice content cannot be unambiguously broken down into cloud ice and snowwhich is why~~ latter can usually not be diagnosed in models which treat snow formation diagnostically. The new single category ice scheme used in this study only predicts the total stratiform ice water content, including snow. Therefore TIWC is most ~~representative~~meaningful for a comparison with this model in the extra-tropics where the contribution from convective snow is rather small. The reference model predicts stratiform cloud ice explicitely but ~~represents snow as a~~ diagnoses the snow mass flux. Therefore we can make full use of the distinction by Li et al. (2012) and compare the reference model to CIWC.

Comparing the different simulations of the new scheme, we see that the 2M and 4M simulations are very similar both in terms of ice water content profiles (top row) and ice water path (TIWP and CIWP respectively; bottom). ~~This suggests~~ The effect of riming on the ice crystal properties is most evident in the mid-latitudes. There, the 4M configuration produces rimed or partially rimed particles with higher fall speeds which results in a reduced ice water content in the lower atmosphere (below roughly $700\,\mathrm{hPa}$) as compared to the 2M configuration where riming does not affect particle properties and thus fall speeds. However, the overall similarities suggest that the increased computational cost of the 4M configuration (see Table 2) and parameterization complexity (4 versus 2 prognostic ice moments) do not significantly improve the overall representation of cloud ice in the GCM.

As explained in Sect. 2, the new cloud cover parameterization couples the cloud fraction to the ice water content. The aggregation parameterization depends on the concentration of ice crystals $S_{agg} \propto N_i^2$, which in turn is computed from the grid-box mean value as $N_i = \overline{N}_i b^{-1}$, i.e. $S_{agg} \propto b^{-2}$. We denote the parameterized source and sink terms by $S_\bullet = (\partial_t q_i)_\bullet$ i.e. the partial time derivative ∂_t of cloud ice q_i restricted to one process. This leads to an artificial feedback loop: Aggregation reduces N_i, increases ice particle size, fall speed and thus the sedimentation sink. Because cloud ice is linked to cloud cover (see the definition of s_1 in Table 1 which replaces s_w in Eq. (1) in the new cloud cover parameterization) the sedimentation of cloud ice decreases the cloud fraction b which in turn increases the in-cloud N_i and the ice crystal aggregation rate S_{agg} artificially. This feedback is the main contributor to the overall slightly lower ice water contents in 2M simulation as compared to the LIM_ICE simulation, which does not have this feedback, and outweighs the effect from the additional humidity that is available for ice growth in the 2M simulation. We acknowledge the existence of this artificial ~~feedback~~ increase of the in-

cloud N_i by sedimentation and the resulting feedback, but do not consider it to be important enough to sacrifice the physical correctness of the method used in the 2M configuration.

The most prominent differences between our simulations and the observations are in the tropics. As can be seen from Table 3, two thirds of the entire surface precipitation is produced by the convective scheme. Since convective precipitation is a diagnostic quantity which is not included in the total ice water content here, a direct comparison of modeled, stratiform IWC/IWP with the observations is limited. With that in mind, we find that the ~~models underestimates the~~ 2M and 4M configurations of the new model underestimate the observed TIWP by roughly a factor of 3 in the tropics ~~.~~ (Fig. 5). This is true for both the new model and the reference model (which has to be compared to CIWP/CIWC). ~~Slightly higher~~ Higher values for TIWP are produced by the LIM_ICE and HET_CIR simulations. While the slightly higher values in the LIM_ICE simulation are due to the cloud fraction - sedimentation feedback explained above, the ~~higher~~ IWC values in the HET_CIR simulations are almost twice as large as in the 2M/4M configurations and are a result of the lower ice supersaturation needed for ice crystals to nucleate heterogeneously. This allows for a ~~slightly~~ more frequent formation of ice clouds at cold temperatures.

In the extra-tropics, the stratiform IWC is more representative of the observed TIWC/TIWP and we find slightly better agreement between the models and observations ~~.~~ (Fig. 5). The vertical profile of TIWC in the mid- and high latitudes is not reproduced by the new model in any configuration, a feature shared with many CMIP5 models (Li et al., 2012), while the reference model performs rather well and only slightly underestimates the ice water path in mid-latitudes. ~~As we will see in Sect. 5, the misrepresentation of the ice mass profile is likely due to unrealistic ice formation pathways in the new model.~~

On the basis of the evaluation above, we choose the 2M configuration as default for the new model for its computational efficiency compared to the 4M configuration and physical correctness compared to the LIM_ICE configuration. Heterogeneous nucleation of ice crystals at low ice supersaturation in the cirrus regime (parameterized in the HET_CIR configuration) can be included optionally for future work with the new model and yields promising results but is not used for the analysis in Sects. 4 and 5 since ~~its~~ it's in part based on unpublished work.

3.5 Cloud liquid water

We compare the simulations with the new and the reference model to the Multisensor Advanced Climatology of Liquid Water Path (MAC-LWP) ~~(Elsaesser et al., 2017)~~(O'Dell et al., 2008; Elsaesser et al., 2017), see Fig. 6. Microwave sensors cannot reliably distinguish precipitation from cloud water. Therefore we only evaluate regions with low precipitation, i.e. where the liquid water (LWP) and total water path (TWP) have similar magnitude. We use the threshold $LWP/TWP > 0.8$ suggested by Elsaesser et al. (2017). The differences in liquid water are very small for the different configurations of the new model, so we only ~~look at~~ evaluate the default configuration 2M. We find an overall high bias in LWP in the extra-tropics for both models but a more pronounced effect in the new model. As discussed above, the TOA energy balance constraints in the new model require a lower tuning parameter for the autoconversion of cloud droplets to rain (γ_r) and thus thicker liquid clouds that reflect more SW radiation. We consider this the main reason for the higher liquid water path in the 2M as compared to the REF simulation, ~~consistent with the findings of Lohmann and Neubauer (2018),~~ as the warm phase parameterizations are the same in both models.

In the Southern Ocean, the overestimation of LWP translates into an overestimation of the SW CRE, evident from the top right panel in Fig. 4. Note that the ~~reference model~~ REF simulation with a smaller positive LWP bias overestimates SW CRE less.

3.6 Cloud phase partitioning

~~The CALIPSO-GOCCP product offers deeper insight into~~ We examine the cloud phase ~~partitioning. Evaluating our modelsagainst this satellite retrieval reveals a significant shortcoming of the new as well as the reference model. We compute the frequency of occurrence of the cloud phase ratio , defined as the fractional contribution of cloud ice~~ ratio (PR; relative fraction of ice clouds to total clouds) to - temperature (T) histograms used in the model-intercomparison by Cesana et al. (2015) (their Fig. 10) in Fig. 7 to assess the realism of the simulated cloud phase partitioning in our models. As has been discussed in Cesana et al. (2015), the satellite product is not directly comparable to model output. Here we use the COSP simulator introduced in the previous sections to maximize comparability. In essence, there are three differences between the datasets that one needs to keep in mind:

First, the phase discrimination of the satellite product is based on a threshold value for the backscattered polarization ratio to separate ice-dominated from liquid-dominated pixels (Cesana and Chepfer, 2013). Second, the resolution of the lidar on board of CALIPSO has a spatial resolution of $333\,\mathrm{m}$. This is much smaller than the model grid with a spacing of roughly $100\,\mathrm{km}$. While the model reports the mass phase ratio (MPR), i.e. the ratio of the ice mass mixing ratio to the total cloud water ~~content, shown in Fig.7. This metric is equivalent to Cesana et al. (2015) who present a comprehensive model inter-comparison of the phase ratio occurrence frequency~~mass mixing ratio within one grid box, the satellite product reports the frequency phase ratio (FPR), i.e. the relative frequency of icy pixels to all cloudy pixels within a $2°$ by $2°$ grid box. Third, the lidar attenuates at a cloud optical thickness above 3 (Cesana et al., 2015).

The different configurations of the new model have very similar PR-T histograms, which is why we only show the one for 2M. For the new model we only count cloudy regions, i.e. require $b > 0$, to exclude falling ice (snow) with ~~a phase ratio of 1.~~

~~Both models capture the pronounced bimodality of the cloud phase distribution but significantly overestimate the frequency of ice cloud occurrence~~ $PR = 1$. Comparing the 2M to the REF simulation in Fig. 7 shows that the 2M simulation produces slightly less supercooled liquid clouds at warm temperatures ~~(and underestimate liquid cloud occurrence at cold temperatures). A whole family of models have a similar issue, as assessed by Cesana et al. (2015). This clearly suggests that there is a systematic error in the parameterization of cloud ice , the freezing process and ice growth in many models . To find the cause for this misrepresentation of the phase ratio, we present a novel approach to diagnose the cloud formation pathways in the next Section~~above $-15\,°\mathrm{C}$ but slightly more at temperatures below $-15\,°\mathrm{C}$. In contrast to REF, where any ice above $0\,°\mathrm{C}$ melts instantly, the 2M employs a finite melting rate which allows for cloud ice at temperatures warmer than $0\,°\mathrm{C}$. In the CALIPSO-GOCCP dataset a temperatures correction is applied so that all clouds at temperatures warmer than $0\,°\mathrm{C}$ are considered liquid.

We can see from Fig. 7 that mixed-phase states are rare in both the models and the satellite observations. For the models this implies that the coexistence of liquid water and ice is rare. For the satellite product it implies that cloud phase is spatially

uniform on the scales of $2°$ by $2°$. The average phase ratio per temperature bin therefore roughly quantifies the relative frequency of pure ice clouds.

In Fig. 8 we present the phase ratio from a simulation using the COSP lidar simulator to assess the differences between model output and the satellite product due to differences in the sampling methods and lidar attenuation. We show the phase ratio of three different datasets: the CALIPSO-GOCCP satellite product, direct model output and the simulated satellite retrieval using COSP. The simulated satellite retrieval is much closer to its measured counterpart than the direct model output. The phase ratio seems to be slightly underestimated at temperatures colder than roughly $-15\,°\mathrm{C}$ and slightly overestimated at temperatures warmer than $-15\,°\mathrm{C}$.

4 Quantifying the ~~cloud~~ ice formation pathways

The microphysical properties of a cloud are defined by the cloud formation processes, i.e. the cloud is simply the product of its formation history. Traditionally, model output reveals a snapshot of the simulated cloud field at any given time. Due to the finite storage capacity, aggregates of the model states are stored and information on the integration from process rates is lost. Most common are temporal averages (e.g. monthly or yearly mean values) or vertical aggregates (e.g. burden, total cloud cover, TOA and surface radiative fluxes or precipitation). The aggregated cloud states are then compared to observations to infer information about the microphysical parameterizations leading to the cloud state. ~~This last step provides significant uncertainty, is unnecessary and ultimately~~ Inferring the dominant processes responsible for a model-to-observation mismatch is difficult. Usually it is very time consuming because many sensitivity studies are necessary where processes are turned off individually and even then the interaction and competition between processes cannot be assessed. Ultimately, spatio-temporally averaged model output defeats the purpose of simulating any physical system: finding cause-and-effect between differential equations and observables.

In this section we tackle the problem the other way around. Instead of inferring the formation history based on the current cloud state, we make use of additional prognostic equations to store and quantify ~~cloud~~ ice formation pathways. This information can then be used to compute conditional probabilities to provide a sound cause-and-effect relation between the microphysical parameterizations and the resulting cloud state. This analysis makes direct inference from observables on cloud microphysical parameterizations tangible.

Our model parameterizes three fundamentally different source terms for cloud ice: Heterogeneous contact and immersion freezing of cloud droplets in the mixed-phase regime $S_{het-frz}$, homogeneous freezing of cloud droplets $S_{hom-frz}$ and nucleation of ice from deliquesced aerosols S_{nuc}. The latter two processes are restricted to temperatures below $-35\,°\mathrm{C}$ while heterogeneous freezing dominates at warmer temperatures. Note that we focus on the mixed-phase regime and thus do not further separate heterogeneous from homogeneous ice nucleation in the cirrus regime, even though nucleation of cloud ice on mineral dust is implemented in the HET_CIR configuration.

To distinguish ice that formed by either of the process rates above, we introduce two additional prognostic tracers to keep track of the formation history of the cloud mass at any given time in the simulation.

4.1 Mixed-phase heterogeneous freezing origin mass fraction

To separate cloud ice that formed in the mixed-phase temperature regime we introduce the heterogeneously nucleated ice mass mixing ratio $q_{i,het}$ governed by the following equation:

$$\partial_t q_{i,het} = S_{het-frz} - v_m \partial_z q_{i,het} + F_{het} \left(S_{col} + S_{dep} - S_{sub} \right). \tag{5}$$

The growth of this tracer depends on the ice mass source and sink terms for collisions with cloud droplets S_{col}, vapor deposition S_{dep}, sublimation S_{sub} and the fraction of cloud ice has already formed previously by heterogeneous freezing, defined as $F_{het} = q_{i,het}/q_i$. We abbreviate the partial derivative with respect to the vertical dimension z (in m) by ∂_z. The tracer sediments along with the total ice mass with the mass-weighted terminal velocity v_m in $\mathrm{m\,s^{-1}}$. Convectively detrained ice is missing here due to a lack of an explicit, aerosol dependant freezing parameterization in the convection scheme. Water is only detrained as ice below temperatures of $-35\,^{\circ}\mathrm{C}$ where we assume that liquid water freezes homogeneously.

4.2 Liquid origin mass fraction

We further distinguish between cloud ice that forms via homogeneous freezing of cloud droplets and ice that nucleates in situ from deliquesced aerosol. This allows to disentangle in situ cirrus from liquid origin cirrus. To quantify the ice mass fraction initiated through freezing of liquid water, we implement a tracer $q_{i,liq-o}$ governed by the following equation:

$$\partial_t q_{i,liq-o} = S_{het-frz} + S_{ice-cv} + S_{hom-frz} - v_m \partial_z q_{i,liq-o} + F_{liq-o} \left(S_{col} + S_{dep} - S_{sub} \right). \tag{6}$$

We sum up all liquid to ice mass source terms, namely homogeneous freezing of cloud droplets $S_{hom-frz}$ and convective detrainment of cloud ice S_{ice-cv} together with the processes defined above. The liquid origin mass fraction is given by $F_{liq-o} = q_{i,liq-o}/q_i$.

4.3 Cloud types based on the cloud formation history

The additional information on the cloud formation history from Eqs. (5) and (6) can be combined with the liquid fraction $F_{liq} = q_l/(q_i + q_l)$, cloud vertical thickness $\Delta p = p_{base} - p_{top}$, i.e. the pressure difference between cloud base p_{base} and cloud top p_{top}, and cloud top temperature T_{top} to build an inclusive set of cloud types. As is evident from Fig. 7, mixed-phase clouds are unstable due to the WBF process, leading to a strongly bimodal distribution of the frequency of phase ratio occurrence. This bimodality exists but is less pronounced for the ice mass source fractions F_{het} and F_{liq-o} shown in Fig. 9 together with the liquid fraction F_{liq}. Ice source mass fractions between zero and one arise from competing formation mechanisms and mixing of clouds of distinct sources.

We make use of the separation of cloud occurrence frequency in the 5-dimensional parameter space (F_{liq}, Δp, F_{het}, F_{liq-o}, T_{top}) to classify clouds into the types defined in Table 4. The labels are based on the analysis of the temperature regime each cloud primarily occurs in and are discussed in more detail below.

The classification is computed online and thus allows to accumulate statistics per cloud type. Examples of such statistics are the cloud top temperature, liquid fraction and liquid origin fraction distributions per cloud type shown in Fig. 10. These

distributions allow to identify physical properties of each cloud type and its associated formation pathway. Below we use them to justify the cloud type labels in Table 4.

Homogeneously nucleated clouds are separated into three classes. They are labeled *cirrus* if they are thinner than $500\,\mathrm{hPa}$, otherwise we refer to them as *thick*. This name ~~stems~~ arises from the fact that the vast majority of such clouds have cloud tops that are colder than $-35\,^{\circ}\mathrm{C}$ as can be seen from the top panel in Fig. 10. We further differentiate between *in situ* cirrus, clouds that nucleated from deliquesced aerosols or formed heterogeneously below $-35\,^{\circ}\mathrm{C}$ in the case of the HET_CIR simulation (not shown), and *liquid origin* cirrus, clouds that formed from homogeneous freezing of cloud droplets. While there is a clear peak for clouds that formed without any liquid water precursors ($F_{liq-o} = 0$), the peak for complete liquid origin clouds $F_{liq-o} = 1$ is less pronounced due to competing primary ice source terms (Fig. 10, bottom panel).

Heterogeneously nucleated clouds are separated into two classes. We find two distinctly different cloud types where ice formed predominantly from heterogeneous freezing of cloud droplets. As shown in Figs. 7 and 9, a truly mixed state with liquid water and ice is unstable and thus rare. Therefore we divide heterogeneously nucleated clouds into those that are dominated by liquid water and ice respectively, see middle panel in Fig. 10. We label them both as *mixed-phase* (*liquid* and *ice dominated* respectively) since the cloud tops of such clouds are predominantly found in the mixed-phase temperature regime between $0\,^{\circ}\mathrm{C}$ and $-35\,^{\circ}\mathrm{C}$.

Liquid clouds are further separated into those with *cold* cloud tops ($T < 0\,^{\circ}\mathrm{C}$) and *warm* cloud tops ($T > 0\,^{\circ}\mathrm{C}$).

In the following sections we will use the cloud types and associated formation pathways described here to gain insights into the simulated cloud fields. It is crucial to keep in mind that the labels provided for the cloud types here ~~area~~ are based on formation pathways. This is in strong contrast to the traditional definitions based exclusively on the cloud state and can thus lead to results that seem counterintuitive at first. For example, cirrus clouds are commonly defined as clouds with temperatures colder than $-35\,^{\circ}\mathrm{C}$ (or more generally the temperature below which homogeneous freezing becomes efficient, depending on the model). Here we only require cirrus clouds to form by the processes that are typically found at temperatures below $-35\,^{\circ}\mathrm{C}$ and subsequently track their evolution without imposing strict temperature constraints. This means however, that a cirrus cloud is still called cirrus, even if its constituent ice crystals fall far into the mixed-phase regime.

5 The ice formation pathways in ECHAM-HAM

We implemented the additional prognostic tracers needed to quantify ice formation pathways introduced in the last Section in the new model. Along with the new microphysics scheme we introduced a new code structure which removed the sequential computation of microphysical tendencies in the reference model and clearly segregates the computation of microphysical tendencies and local model state updates (Dietlicher et al., 2018). This allows to easily implement additional tracers. Although we did not implement the same tracers in the reference model as well, we expect that the insights gained from this Section can be transferred to the reference model since many aspects of the model are the same or very similar, e.g. the diffusion, convection and cloud cover parametrizations (except in the cirrus regime).

With the additional prognostic equations to identify ~~cloud~~ ice formation pathways and the cloud types derived thereof, we are able find the microphysical ~~cause~~ causes for the macrophysical cloud ~~state~~ states simulated by the new model. ~~Identifying unrealistic cloud formation pathways allows to directly target faulty microphysical parameterizations or define tuning targets.~~ A clear causal relationship between the simulated cloud fields and the underlying parametrizations is critical for model development. Improving the representation of sub-grid processes is usually a two-step process: First, observational data is used to evaluate the simulated cloud fields and then model sensitivities are assessed to find the parametrizations responsible for potential model-to-observation mismatches. In the following we demonstrate how the ice formation pathways introduced in the last Section can be used for the second step using the example of the phase ratio discussed in Sect. 3 and Fig. 7.

5.1 Relative cloud type frequencies

We classify the clouds online according to Table 4 to generate a global climatology of the relative contributions of each formation pathway to the 3D cloud volume (defined as the air mass covered by the cloud) in Fig. 11. From this pie chart it is evident that the majority of the cloud population consists of homogeneously nucleated ice clouds (in situ cirrus and thick clouds) and liquid clouds. The next smaller class are the liquid origin cirrus clouds, making up almost $11\,\%$ of the cloud population or almost one ~~fourth~~ third of all cirrus clouds. Mixed-phase clouds only contribute roughly $5\,\%$, with the fraction of such clouds that are dominated by ice ~~water~~ being smaller than those being dominated by liquid water.

We also show ~~a more detailed map of~~ zonal means of the cloud type occurrence ~~frequency~~ frequencies in Fig. 12. This view sheds more light on where each formation pathway dominates. Liquid clouds with warm cloud tops dominate in the tropics while their cold top counterparts are primarily found in mid-latitudes. Due to abundant deep convection in the tropics, large amounts of liquid water are transported to high altitudes where homogeneous freezing of cloud droplets sets in, leading to a frequent occurrence of liquid origin cirrus clouds. Heterogeneous freezing only affects clouds at low altitudes where there is no competition with homogeneous nucleation. Seemingly inexistent are mixed-phase clouds where heterogeneous freezing of cloud droplets alone causes glaciation of the host liquid cloud.

5.2 ~~The mixed-phase ice overestimation~~Decomposing the cloud phase partitioning

~~The absolute frequency of occurrence of cloud types shown in the top panel in~~ By sampling the cloud types according to temperature we find the dominant parametrizations controlling the phase ratio in our model. Fig. 13 ~~reveals the pathways responsible for the global mean overestimation of the ice fraction in the mixed-phase regime as compared to the CALIPSO-GOCCP product (discussed above and shown in Fig. 7).~~ shows the absolute frequency of occurrence of each cloud type in the top panel. The most frequent cloud types simulated in the mixed-phase regime are thick clouds, in situ cirrus, liquid origin cirrus and only then followed by the two heterogeneously nucleated cloud types. The fact that we find homogeneously nucleated clouds with a vertical extent of less than $500\,\mathrm{hPa}$ (i.e. cirrus clouds) down to temperatures of $0\,^{\circ}\mathrm{C}$ is in part due to the choice of the threshold value to separate cirrus clouds from thick clouds but does not affect the main conclusion: The dominant source term for cloud ice in the mixed-phase temperature regime is homogeneous freezing of deliquesced aerosols taking place at temperatures below $-35\,^{\circ}\mathrm{C}$.

Analogously to the prognostic tracers introduced in Sect. 4 and formally defined in Eq. (A1), we trace the state of water from which ice forms. The frozen liquid ice mass mixing ratio tracer accumulates the mass of liquid water that has been converted to ice by freezing, riming or the WBF process and allows to compute the frozen liquid fraction as $F_{liq-f} = q_{i,liq-f}/q_i$. For the majority of homogeneously nucleated clouds, the frozen liquid fraction is very small ($< 10\,\%$) from which we conclude that ice predominantly forms directly from deposition of water vapor (excluding the WBF process) and thus without a liquid water precursor, see the bottom panel in Fig. 13. ~~We conclude that homogeneously nucleated ice~~ This implies that ice nucleated in the cirrus regime not only dominates ~~the frequency of occurrence of ice in the~~ glaciation in mixed-phase ~~regime~~ clouds but also inhibits the formation of ~~liquid clouds and thus heterogeneously nucleating ice clouds by quickly taking up any liquid water encountered on the fall-trajectory of the ice crystals, making vapor deposition the main ice growth term.~~ supercooled liquid water clouds. As a result, contact and immersion freezing is limited to clouds with cloud tops warmer than $-35\,^{\circ}\mathrm{C}$ where there is no competition with sedimenting ice that formed in the cirrus regime.

~~This offers two explanations for the differences between the modeled phase ratio and the CALIPSO-GOCCP product. Either the model produces too many thick clouds or the satellite is not able to detect the vertical extent of such clouds due to attenuation and therefore underestimates the frequency of ice occurrence at warmer temperatures.~~

~~We can think of four mechanisms that lead to an overestimation of thick clouds in the model, listed in descending likelihood according to our judgment: This analysis reveals unequivocally that the overestimation of cloud ice~~ The frequency of ice clouds in the mixed-phase regime ~~and the underestimation of super-cooled liquid water cannot be associated with~~ seen in Figs. 7 and 8 cannot be attributed to heterogeneous freezing and ~~ice growth~~ the WBF process in the mixed-phase regime itself but is ~~due to homogenous~~ instead a result of homogeneous freezing and subsequent sedimentation of ice ~~at colder~~ from colder temperatures into the mixed-phase regime. The clouds belonging to the thick category have a large vertical extent and therefore also substantial optical thickness (a majority is above 60, not shown). This explains the large difference between the two different phase ratio diagnostics in Fig. 8. The satellite simulator misses the lower part of thick clouds due to full attenuation which suppresses the otherwise high frequency of ice clouds at these temperatures.

6 Conclusions

We presented ~~a~~ the global performance of the new cloud microphysics scheme in the ECHAM6-HAM2 GCM introduced in D18. The main ~~improvement over~~ difference as compared to its predecessor is the consistent description of cloud ice using a single, prognostic category. Thus, it does not rely on poorly constrained conversion parameterizations between in-cloud ice and precipitating snow categories. ~~We~~ Different from D18, we introduced a new approach to extend the sub-grid cloud cover scheme of Sundqvist et al. (1989) to ice clouds. This scheme ~~does no longer have~~ no longer has the positive cloud cover bias at temperatures below $-35\,^{\circ}\mathrm{C}$ ~~from~~ present in the reference model~~and therefore allows for smaller, arguably more reasonable tuning parameters~~.

We assessed ~~cloud~~ ice formation pathways quantitatively by introducing additional prognostic equations for the heterogeneously formed and liquid origin ice mass mixing ratios. We found that in our model the majority of cloud ice forms below

$-35\,°C$ by either homogeneous freezing of cloud droplets or homogeneous nucleation of deliquesced aerosols. Only about ~~of the cloud volume is dominated by heterogeneous~~ 5 % of clouds form by contact and immersion freezing in mixed-phase temperatures, making homogeneous freezing (and heterogeneous nucleation of cloud ice on mineral dust at temperatures colder than $-35\,°C$ in the HET_CIR configuration, not shown) the main source for cloud ice even at temperatures warmer than $-35\,°C$. The Lagrangian perspective on the modeled cloud ~~field~~ fields provided by the formation pathway analysis allowed to distinguish in situ and liquid origin cirrus clouds. We found that roughly one ~~forth~~ third of all cirrus clouds form ~~from~~ by homogeneous freezing of cloud droplets.

Furthermore, ~~cloud~~ ice formation pathways provide the causal link between the microphysical parameterizations and the resulting cloud ~~field. With an example for the cloud phase ratio, we showed that this link~~ fields. We showed how they can be used ~~as a powerful tool to use satellite products to pinpoint unrealistic parameterizations. A comparison with the~~ to break the simulated phase ratio down into the contributions of different microphysical parameterizations. We find that mixed-phase processes like the WBF-process and heterogeneous freezing of supercooled cloud droplets play a minor role in our model because most ice originates in the cirrus regime. Differences between the simulated cloud phase ratio and the CALIPSO-GOCCP ~~product revealed that our model underestimates the frequency of occurrence of supercooled liquid water (and overestimates the frequency of cloud ice occurrence) in the mixed-phase regime. Through the analysis of cloud formation pathways we could identify the responsible microphysical parameterizations for this discrepancy. Interestingly, we found that it is not the processes taking place in the~~ satellite product can be explained by differences in the sampling methods between model and satellite and attenuation of the lidar signal. The formation pathways revealed that most of the simulated ice clouds are in the blind spot of the lidar in the lower part of optically thick clouds. This highlights the limited applicability of the CALIPSO-GOCCP dataset to constrain cloud ice at warm mixed-phase ~~regime itself (WBF process, heterogeneous freezing of cloud droplets and riming) which are responsible for this overestimation but rather a combination of ice formation processes at temperatures colder than and subsequent sedimentation. This suggests that model improvements regarding the cloud phase ratio should relax the maximal cloud overlap assumption for sedimentation~~temperatures.

Code availability. The code of the cloud microphysics module (Fortran 95) is available upon request from the corresponding author or as part of the ECHAM6-HAMMOZ chemistry climate model through the HAMMOZ distribution web-page https://redmine.hammoz.ethz.ch/projects/hammoz.

Competing interests. The authors declare that they have no conflict of interest.

Acknowledgements. This project has been funded by the Swiss National Science Foundation (project number 200021_160177). The ECHAM-HAMMOZ model is developed by a consortium composed of ETH Zurich, Max Planck Institut für Meteorologie, Forschungszentrum Jülich, University of Oxford, the Finnish Meteorological Institute and the Leibniz Institute for Tropospheric Research, and managed by the Center

for Climate Systems Modeling (C2SM) at ETH Zurich. Special thanks go to Sylvaine Ferrachat for technical support regarding the model. The computing time for this work was supported by a grant from the Swiss National Supercomputing Center (CSCS) under project ID s652 and from ETH Zurich. We thank Steffen Münch for providing his implementation of a more advanced cirrus parameterizations for the sensitivity tests presented here. We obtained the CERES EBAF data from the NASA Langley Research Center CERES ordering tool at http://ceres.larc.nasa.gov/. The GPCP data has been provided by the NOAA-ESRL Physical Sciences Division, Boulder Colorado from their Web site at https://www.esrl.noaa.gov/psd/. Finally, we express our gratitude to the two anonymous reviewers for their useful comments.

Appendix A: ~~Additional prognostic equations to diagnose cloud formation~~Frozen liquid mass fraction

A1 ~~Frozen liquid mass fraction~~

We do not only diagnose the phase which initiated ice formation to separate liquid origin from vapor origin ice but also keep track of the total amount of liquid water that has been converted to ice with a separate tracer $q_{i,liq-f}$, the mass mixing ratio for frozen liquid water defined as:

$$\partial_t q_{i,liq-f} = S_{het-frz} + S_{ice-cv} + S_{hom-frz} + S_{col} - v_m \partial_z q_{i,liq-o} - F_{liq-f} S_{sub}. \quad \text{(A1)}$$

Analogous to the tracers defined in ~~Section 4~~Sect. 4, we define the frozen liquid fraction as $F_{liq-f} = q_{i,liq-f}/q_i$. ~~The difference to the liquid origin mass fraction is that deposition is not taken into account.~~

In contrast to the these tracers defined previously, the frozen liquid water mass mixing ratio contains information on ice growth history rather than source processes.

References

Adler, R. F., Sapiano, M. R. P., Huffman, G. J., Wang, J.-J., Gu, G., Bolvin, D., Chiu, L., Schneider, U., Becker, A., Nelkin, E., Xie, P., Ferraro, R., and Shin, D.-B.: The Global Precipitation Climatology Project (GPCP) Monthly Analysis (New Version 2.3) and a Review of 2017 Global Precipitation, Atmosphere, 9, doi:10.3390/atmos9040138, 2018.

Ansmann, A., Tesche, M., Knippertz, P., Bierwirth, E., Althausen, D., Müller, D., and Schulz, O.: Vertical profiling of convective dust plumes in southern Morocco during SAMUM, Tellus B, 61, 340–353, doi:10.1111/j.1600-0889.2008.00384.x, 2009.

Atkinson, J. D., Murray, B. J., Woodhouse, M. T., Whale, T. F., Baustian, K. J., Carslaw, K. S., Dobbie, S., O'Sullivan, D., and Malkin, T. L.: The importance of feldspar for ice nucleation by mineral dust in mixed-phase clouds, Nature, 498, 355–358, doi:10.1038/nature12278, 2013.

Austin, R. T., Heymsfield, A. J., and Stephens, G. L.: Retrieval of ice cloud microphysical parameters using the CloudSat millimeter-wave radar and temperature, J. geophys. res-atmos., 114, doi:10.1029/2008JD010049, 2009.

Bodas-Salcedo, A., Webb, M. J., Bony, S., Chepfer, H., Dufresne, J.-L., Klein, S. A., Zhang, Y., Marchand, R., Haynes, J. M., Pincus, R., and John, V. O.: COSP: Satellite simulation software for model assessment, B. am. meteorol. soc., 92, 1023–1043, doi:10.1175/2011BAMS2856.1, 2011.

Bodas-Salcedo, A.: Cloud Condensate and Radiative Feedbacks at Midlatitudes in an Aquaplanet, Geophys. res. lett., 45, 3635–3643, doi:10.1002/2018GL077217, 2018.

Boucher, O., Randall, D., Artaxo, P., Bretherton, C., Feingold, G., Forster, P., Kerminen, V.-M., Kondo, Y., Liao, H., Lohmann, U., Rasch, P., Satheesh, S., Sherwood, S., Stevens, B., and Zhang, X.: Clouds and Aerosols, book section 7, p. 571–658, Cambridge University Press, Cambridge, United Kingdom and New York, NY, USA, doi:10.1017/CBO9781107415324.016, www.climatechange2013.org, 2013.

Ceppi, P., Hartmann, D. L., and Webb, M. J.: Mechanisms of the Negative Shortwave Cloud Feedback in Middle to High Latitudes, J. climate, 29, 139–157, doi:10.1175/JCLI-D-15-0327.1, 2016.

Cesana, G. and Chepfer, H.: Evaluation of the cloud thermodynamic phase in a climate model using CALIPSO-GOCCP, J. geophys. res-atmos., 118, 7922–7937, doi:10.1002/jgrd.50376, 2013.

Cesana, G., Waliser, D. E., X., J., and F., L. J.: Multimodel evaluation of cloud phase transition using satellite and reanalysis data, J. geophys. res-atmos., 120, 7871–7892, doi:10.1002/2014JD022932, 2015.

Delanoë, J. and Hogan, R. J.: A variational scheme for retrieving ice cloud properties from combined radar, lidar, and infrared radiometer, Journal of Geophysical Research: Atmospheres, 113, doi:10.1029/2007JD009000, https://agupubs.onlinelibrary.wiley.com/doi/abs/10.1029/2007JD009000, 2008.

Delanoë, J. and Hogan, R. J.: Combined CloudSat-CALIPSO-MODIS retrievals of the properties of ice clouds, Journal of Geophysical Research: Atmospheres, 115, doi:10.1029/2009JD012346, https://agupubs.onlinelibrary.wiley.com/doi/abs/10.1029/2009JD012346, 2010.

DeMott, P. J., Prenni, A. J., McMeeking, G. R., Sullivan, R. C., Petters, M. D., Tobo, Y., Niemand, M., Möhler, O., Snider, J. R., Wang, Z., and Kreidenweis, S. M.: Integrating laboratory and field data to quantify the immersion freezing ice nucleation activity of mineral dust particles, Atmos. chem. phys., 15, 393–409, doi:10.5194/acp-15-393-2015, 2015.

Deng, M., Mace, G. G., Wang, Z., and Lawson, R. P.: Evaluation of Several A-Train Ice Cloud Retrieval Products with In Situ Measurements Collected during the SPARTICUS Campaign, Journal of Applied Meteorology and Climatology, 52, 1014–1030, doi:10.1175/JAMC-D-12-054.1, 2013.

Dietlicher, R., Neubauer, D., and Lohmann, U.: Prognostic parameterization of cloud ice with a single category in the aerosol-climate model ECHAM(v6.3.0)-HAM(v2.3), Geoscientific Model Development, 11, 1557–1576, doi:10.5194/gmd-11-1557-2018, 2018.

Eidhammer, T., Morrison, H., Mitchell, D., Gettelman, A., and Erfani, E.: Improvements in Global Climate Model Microphysics Using a Consistent Representation of Ice Particle Properties, J. climate, 30, 609–629, doi:10.1175/JCLI-D-16-0050.1, 2017.

Elsaesser, G. S., O'Dell, C. W., Lebsock, M. D., Bennartz, R., Greenwald, T. J., and Wentz, F. J.: The Multisensor Advanced Climatology of Liquid Water Path (MAC-LWP), J. climate, 30, 10 193–10 210, doi:10.1175/JCLI-D-16-0902.1, 2017.

Fan, J., Ghan, S., Ovchinnikov, M., Liu, X., Rasch, P. J., and Korolev, A.: Representation of Arctic mixed-phase clouds and the Wegener-Bergeron-Findeisen process in climate models: Perspectives from a cloud-resolving study, J. geophys. res-atmos., 116, doi:10.1029/2010JD015375, 2011.

Flato, G., Marotzke, J., Abiodun, B., Braconnot, P., Chou, S. C., Collins, W., Cox, P., Driouech, F., Emori, S., Eyring, V., Forest, C., Gleckler, P., Guilyardi, E., Jakob, C., Kattsov, V., Reason, C., and Rummukainen, M.: Evaluation of climate models, pp. 741–882, Cambridge University Press, Cambridge, UK, doi:10.1017/CBO9781107415324.020, 2013.

Frey, W. R. and Kay, J. E.: The influence of extratropical cloud phase and amount feedbacks on climate sensitivity, Clim. dyn., 50, 3097–3116, doi:10.1007/s00382-017-3796-5, 2018.

Gasparini, B., Meyer, A., Neubauer, D., Münch, S., and Lohmann, U.: Cirrus Cloud Properties as Seen by the CALIPSO Satellite and ECHAM-HAM Global Climate Model, J. climate, 31, 1983–2003, doi:10.1175/JCLI-D-16-0608.1, 2018.

Gettelman, A., Liu, X., Ghan, S. J., Morrison, H., Park, S., Conley, A. J., Klein, S. A., Boyle, J., Mitchell, D. L., and Li, J. L. F.: Global simulations of ice nucleation and ice supersaturation with an improved cloud scheme in the Community Atmosphere Model, J. geophys. res-atmos., 115, doi:10.1029/2009JD013797, 2010.

Hande, L. B. and Hoose, C.: Partitioning the primary ice formation modes in large eddy simulations of mixed-phase clouds, Atmos. phem. phys., 17, 14 105–14 118, doi:10.5194/acp-17-14105-2017, https://www.atmos-chem-phys.net/17/14105/2017/, 2017.

Hogan, R. J.: Fast approximate calculation of multiply scattered lidar returns, Appl. Opt., 45, 5984–5992, doi:10.1364/AO.45.005984, 2006.

Hoose, C., Kristjánsson, J. E., Chen, J.-P., and Hazra, A.: A Classical-Theory-Based Parameterization of Heterogeneous Ice Nucleation by Mineral Dust, Soot, and Biological Particles in a Global Climate Model, J. atmos. sci., 67, 2483–2503, doi:10.1175/2010JAS3425.1, 2010.

Ickes, L., Welti, A., Hoose, C., and Lohmann, U.: Classical nucleation theory of homogeneous freezing of water: thermodynamic and kinetic parameters, Phys. chem. chem. phys., 17, 5514–5537, doi:10.1039/c4cp04184d, 2015.

Jakob, C. and Tselioudis, G.: Objective identification of cloud regimes in the Tropical Western Pacific, Geophys. res. lett., 30, doi:10.1029/2003GL018367, https://agupubs.onlinelibrary.wiley.com/doi/abs/10.1029/2003GL018367, 2003.

Kanji, Z. A., Ladino, L. A., Wex, H., Boose, Y., Burkert-Kohn, M., Cziczo, D. J., and Krämer, M.: Overview of Ice Nucleating Particles, Meteorol. monogr., 58, 1.1–1.33, doi:10.1175/AMSMONOGRAPHS-D-16-0006.1, 2017.

Kärcher, B., Hendricks, J., and Lohmann, U.: Physically based parameterization of cirrus cloud formation for use in global atmospheric models, J. geophys. res-atmos., 111, doi:10.1029/2005JD006219, 2006.

Komurcu, M., Storelvmo, T., Tan, I., Lohmann, U., Yun, Y., Penner, J. E., Wang, Y., Liu, X., and Takemura, T.: Intercomparison of the cloud water phase among global climate models, J. geophys. res-atmos., 119, 3372–3400, doi:10.1002/2013JD021119, 2014.

Koop, T. B., Luo, B. P., Tsias, A., and Peter, T.: Water Activity as the determinant for homogeneous ice nucleation in aqueous solutions, Nature, 406, 611–4, doi:10.1038/35020537, 2000.

Korolev, A. and Isaac, G.: Phase transformation of mixed-phase clouds, Q. j. roy. meteor. soc., 129, 19–38, doi:10.1256/gj.01.203, 2003.

Krämer, M., Rolf, C., Luebke, A., Afchine, A., Spelten, N., Costa, A., Meyer, J., Zöger, M., Smith, J., Herman, R. L., Buchholz, B., Ebert, V., Baumgardner, D., Borrmann, S., Klingebiel, M., and Avallone, L.: A microphysics guide to cirrus clouds – Part 1: Cirrus types, Atmos. chem. phys., 16, 3463–3483, doi:10.5194/acp-16-3463-2016, 2016.

Li, J.-L. F., Waliser, D. E., Chen, W.-T., Guan, B., Kubar, T., Stephens, G., Ma, H.-Y., Deng, M., Donner, L., Seman, C., and Horowitz, L.: An observationally based evaluation of cloud ice water in CMIP3 and CMIP5 GCMs and contemporary reanalyses using contemporary satellite data, J. geophys. res-atmos., doi:10.1029/2012JD017640, 2012.

Li, Z.-X. and Le Treut, H.: Cloud-radiation feedbacks in a general circulation model and their dependence on cloud modelling assumptions, Climate Dynamics, 7, 133–139, doi:10.1007/BF00211155, 1992.

Loeb, N. G., Doelling, D. R., Wang, H., Su, W., Nguyen, C., Corbett, J. G., Liang, L., Mitrescu, C., Rose, F. G., and Kato, S.: Clouds and the Earth's Radiant Energy System (CERES) Energy Balanced and Filled (EBAF) Top-of-Atmosphere (TOA) Edition-4.0 Data Product, J. clim., 31, 895–918, doi:10.1175/JCLI-D-17-0208.1, 2018.

Lohmann, U. and Neubauer, D.: The importance of mixed-phase clouds for climate sensitivity in the global aerosol-climate model ECHAM6-HAM2, Atmos. chem. phys. discuss., 2018, 1–32, doi:10.5194/acp-2018-97, 2018.

Lohmann, U. and Roeckner, E.: Design and performance of a new cloud microphysics scheme developed for the ECHAM general circulation model, Climate Dynamics, 12, 557–572, doi:10.1007/BF00207939, 1996.

Lohmann, U., Lüönd, F., and Mahrt, F.: An Introduction to Clouds: From the Microscale to Climate, Cambridge University Press, doi:10.1017/CBO9781139087513, 2016.

Marcolli, C.: Pre-activation of aerosol particles by ice preserved in pores, Atmos. chem. phys., 17, 1596–1623, doi:10.5194/acp-17-1595-2017, 2017.

Mauritsen, T., Stevens, B., Roeckner, E., Crueger, T., Esch, M., Giorgetta, M., Haak, H., Jungclaus, J., Klocke, D., Matei, D., Mikolajewicz, U., Notz, D., Pincus, R., Schmidt, H., and Tomassini, L.: Tuning the climate of a global model, J. adv. model. earth sy., 4, doi:10.1029/2012MS000154, 2012.

McCoy, D. T., Tan, I., Hartmann, D. L., Zelinka, M. D., and Storelvmo, T.: On the relationships among cloud cover, mixed-phase partitioning, and planetary albedo in GCMs, J. adv. model. earth sy., 8, 650–668, doi:10.1002/2015MS000589, 2016.

Mitchell, J. F., Senior, C., and Ingram, W.: C02 and climate: a missing feedback?, Nature, 341, 132, 1989.

Morrison, H. and Gettelman, A.: A New Two-Moment Bulk Stratiform Cloud Microphysics Scheme in the Community Atmosphere Model, Version 3 (CAM3). Part I: Description and Numerical Tests, J. climate, 21, 3642–3659, doi:10.1175/2008JCLI2105.1, 2008.

Morrison, H. and Milbrandt, J. A.: Parameterization of Cloud Microphysics Based on the Prediction of Bulk Ice Particle Properties. Part I: Scheme Description and Idealized Tests, J. atmos. sci., 72, 287–311, doi:10.1175/JAS-D-14-0065.1, 2015.

Myhre, G., Shindell, D., Breon, F.-M., Collins, W., Fuglestvedt, J., Huang, J., Koch, D., Lamarque, J.-F., Lee, D., Mendoza, B., Nakajima, T., Robock, A., Stephens, G., Takemura, T., and Zhang, H.: Anthropogenic and Natural Radiative Forcing, book section 8, p. 659–740, Cambridge University Press, Cambridge, United Kingdom and New York, NY, USA, doi:10.1017/CBO9781107415324.018, www.climatechange2013.org, 2013.

Neubauer, D., Lohmann, U., Hoose, C., and Frontoso, M. G.: Impact of the representation of marine stratocumulus clouds on the anthropogenic aerosol effect, Atmos. chem. phys., 14, 11 997–12 022, doi:10.5194/acp-14-11997-2014, 2014.

O'Dell, C. W., Wentz, F. J., and Bennartz, R.: Cloud Liquid Water Path from Satellite-Based Passive Microwave Observations: A New Climatology over the Global Oceans, Journal of Climate, 21, 1721–1739, doi:10.1175/2007JCLI1958.1, 2008.

Stevens, B., Giorgetta, M., Esch, M., Mauritsen, T., Crueger, T., Rast, S., Salzmann, M., Schmidt, H., Bader, J., Block, K., Brokopf, R., Fast, I., Kinne, S., Kornblueh, L., Lohmann, U., Pincus, R., Reichler, T., and Roeckner, E.: Atmospheric component of the MPI-M Earth System Model: ECHAM6, J. adv. model. earth sy., 5, 146–172, doi:10.1002/jame.20015, 2013.

Storelvmo, T., Tan, I., and Korolev, A. V.: Cloud Phase Changes Induced by CO2 Warming—a Powerful yet Poorly Constrained Cloud-Climate Feedback, Curr. clim. change rep., 1, 288–296, doi:10.1007/s40641-015-0026-2, 2015.

Sundqvist, H., Berge, E., and Kristjansson, J.: Condensation and cloud parameterization studies with a mesoscale numerical weather prediction model, Mon. weather rev., 117, 1641–1657, doi:10.1175/1520-0493(1989)117<1641:CACPSW>2.0.CO;2, 1989.

Tan, I., Storelvmo, T., and Zelinka, M. D.: Observational constraints on mixed-phase clouds imply higher climate sensitivity, Science, 352, 224–227, doi:10.1126/science.aad5300, 2016.

Terai, C. R., Klein, S. A., and Zelinka, M. D.: Constraining the low-cloud optical depth feedback at middle and high latitudes using satellite observations, J. geophys. res-atmos., 121, 9696–9716, doi:10.1002/2016JD025233, 2016.

Tsushima, Y., Ringer, M. A., Koshiro, T., Kawai, H., Roehrig, R., Cole, J., Watanabe, M., Yokohata, T., Bodas-Salcedo, A., Williams, K. D., and Webb, M. J.: Robustness, uncertainties, and emergent constraints in the radiative responses of stratocumulus cloud regimes to future warming, Clim. dyn., 46, 3025–3039, doi:10.1007/s00382-015-2750-7, https://doi.org/10.1007/s00382-015-2750-7, 2016.

Welti, A., Kanji, Z. A., Lueoend, F., Stetzer, O., and Lohmann, U.: Exploring the Mechanisms of Ice Nucleation on Kaolinite: From Deposition Nucleation to Condensation Freezing, J. atmos. sci., 71, 16–36, doi:10.1175/JAS-D-12-0252.1, 2014.

Wernli, H., Boettcher, M., Joos, H., Miltenberger, A. K., and Spichtinger, P.: A trajectory-based classification of ERA-Interim ice clouds in the region of the North Atlantic storm track, Geophysical Research Letters, 43, 6657–6664, doi:10.1002/2016GL068922, 2016.

Williams, K. D. and Tselioudis, G.: GCM intercomparison of global cloud regimes: present-day evaluation and climate change response, Clim. dyn., 29, 231–250, doi:10.1007/s00382-007-0232-2, https://doi.org/10.1007/s00382-007-0232-2, 2007.

Williams, K. D. and Webb, M. J.: A quantitative performance assessment of cloud regimes in climate models, Clim. dyn., 33, 141–157, doi:10.1007/s00382-008-0443-1, https://doi.org/10.1007/s00382-008-0443-1, 2009.

Xi, Z., Yanluan, L., Yiran, P., Bin, W., Hugh, M., and Andrew, G.: A single ice approach using varying ice particle properties in global climate model microphysics, J. adv. model. Earth syst., 9, 2138–2157, doi:10.1002/2017MS000952, 2017.

Xu, K.-M. and Krueger, S. K.: Evaluation of Cloudiness Parameterizations Using a Cumulus Ensemble Model, Monthly Weather Review, 119, 342–367, doi:10.1175/1520-0493(1991)119<0342:EOCPUA>2.0.CO;2, 1991.

Zelinka, M. D., Klein, S. A., Taylor, K. E., Andrews, T., Webb, M. J., Gregory, J. M., and Forster, P. M.: Contributions of Different Cloud Types to Feedbacks and Rapid Adjustments in CMIP5, J. climate, 26, 5007–5027, doi:10.1175/JCLI-D-12-00555.1, 2013.

Table 1. The parameters involved in the cloud cover scheme, Eqs. (1) and (4). The rows show different parameters as a function of the temperature regime T. We discuss two different choices for s and Q_i in the text, s_1/$Q_{i,1}$ and s_2/$Q_{i,2}$. We use a linear weighting function $w(T) = (T - 273.15)/(238.15 - 273.15)$ for T in K.

	$T < -35\,^{\circ}\mathrm{C}$	$-35\,^{\circ}\mathrm{C} < T < 0\,^{\circ}\mathrm{C}$	$0\,^{\circ}\mathrm{C} < T$
s_1	$(q_v + q_i)/q_{si}$	$(q_v + q_i)/q_{si}$	q_v/q_{sw}
$Q_{i,1}$	$q_v - q_{si}$	$Q + q_l + (q_v - q_{si})$	$Q + q_l + (q_v - q_{si})$
s_2	$(q_v + q_i)/q_{si}$	q_v/q_{si}	q_v/q_{sw}
$Q_{i,2}$	$q_v - q_{si}$	$Q + q_l$	$Q + q_l$
s_{max}	s_{koop}	q_{si}/q_{sw}	1
s_{min}	1	$w(T) + (1 - w(T))K$	K

Table 2. Description of the model configurations shown in this paper. Tuning parameters are as follows: γ_r is the scaling factor for warm rain formation, f_{fall} is a scaling factor for ice sedimentation speed, γ_s is a scaling parameter for snow formation, e_{ii} is the collision efficiency of ice crystals and γ_{cpr} is the conversion rate from cloud water and ice to precipitation in the convection scheme. Dashes '$-$' denote that those parameters are no longer needed in the new scheme. The last column shows the CPU time for 1 year of simulation relative to the reference model.

Simulation	Description	γ_r	f_{fall}	γ_s	e_{ii}	γ_{cpr} (s^{-1})	CPU time
REF	Reference version: ECHAM6.3-HAM2.3	10.6	3	900	$0.09e^{T_c}$	9×10^{-4}	–
2M	Single category, 2 prognostic ice moments	7	–	–	0.5	2.5×10^{-4}	+29 %
4M	Single category, 4 prognostic ice moments	7	–	–	0.5	2.5×10^{-4}	+41 %
LIM_ICE	As 2M but deposition below $q_v = q_{s,w}$ is shut down for $T > -35\,^{\circ}\mathrm{C}$.	7	–	–	0.5	2.5×10^{-4}	+24 %
HET_CIR	As 2M but with het. nucleation in cirrus regime	9.5	–	–	0.5	1.5×10^{-4}	+24 %

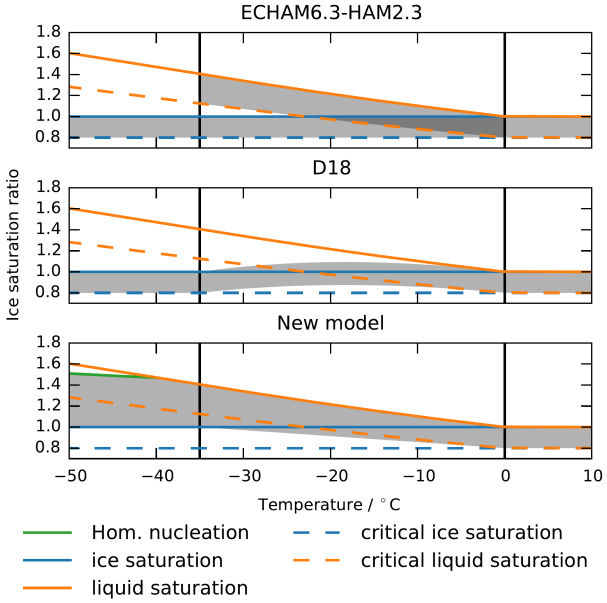

Figure 1. Regions where clouds can form (grey shaded areas) as a function of temperature and supersaturation with respect to ice. The colored lines show liquid water and ice saturation ratios $s_{w/i}$ (solid lines) and the critical saturation ratios required for first cloud formation (dashed; $s_{w/i}K$). We choose a constant $K = 0.8$ for this illustration. The top panel shows the sub-grid cloud scheme of the reference model ECHAM6.3-HAM2.3 which switches between liquid and ice saturation in the mixed-phase regime, the middle panel shows the mixed-saturation approach of Dietlicher et al. (2018) (D18) and the bottom panel shows the new model.

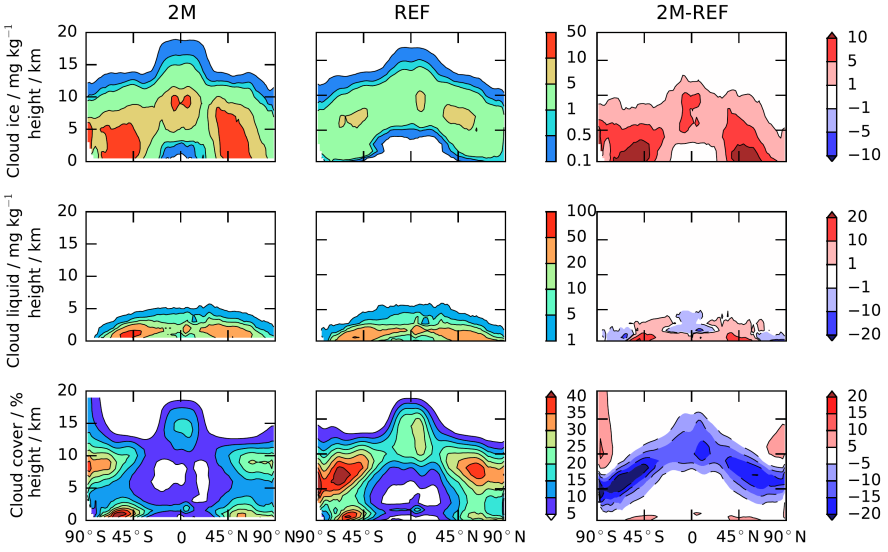

Figure 2. 10-year, zonal mean cloud ice water content (top row), cloud liquid water content (middle row) and cloud cover (bottom row) for the new model (2M configuration; left), the reference model (REF; middle) and differences between the two schemes (right).

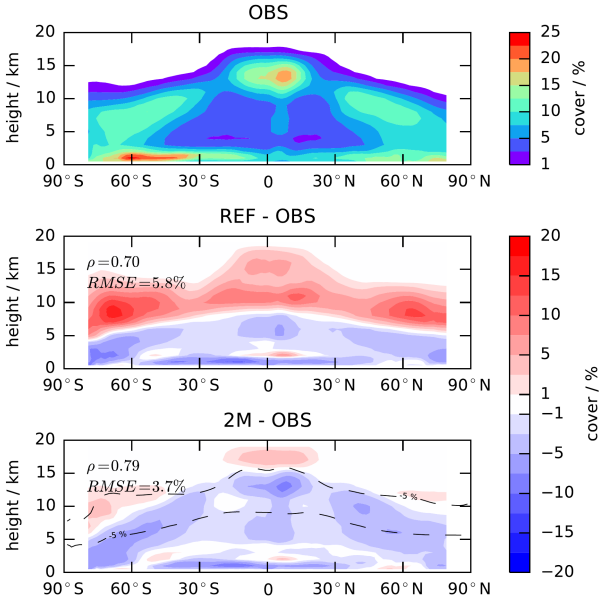

Figure 3. Comparison of the simulated cloud fraction for simulations with the 2M configuration of the new model and the reference model (REF) for 10 years (2003-2012) and the CALIPSO-GOCCP satellite product (day and night, 7 years, 2008-2014). Model output is computed using the COSP-simulator. The Pearson correlation coefficient (ρ) and root mean square error ($RMSE$) of the full, three dimensional cloud cover climatology are computed for both models and shown in the difference plots. The dashed line indicates the area where there is a large (more than $5\,\%$) difference between the 2M and REF simulations as shown in the bottom right panel in Fig. 2.

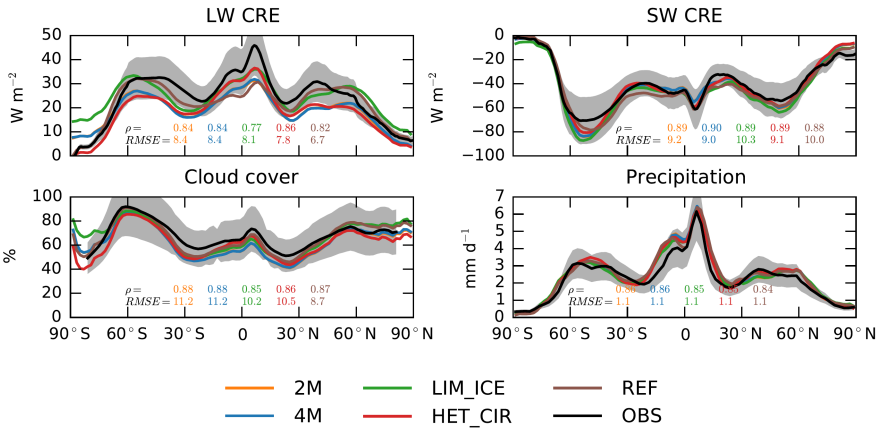

Figure 4. 10-year, zonal mean values for longwave (LW CRE) and shortwave cloud radiative effects (SW CRE) (top row) and total cloud cover and precipitation (bottom row). The colored lines show simulations of different configurations of the new model in Table 2. Black lines show satellite products. For CRE we show data from CERES EBAF (2000 to 2017). Total cloud cover is shown for CALIPSO-GOCCP (2006 to 2012) using the COSP-simulator for the model output. Precipitation data is from the GPCP (2003 to 2012). The interannual spread of the climatologies is represented by $\pm$ one standard deviation (grey). The Pearson correlation coefficient and root mean square error are reported by text in matching colors for the different simulations and computed using the full two dimensional fields.

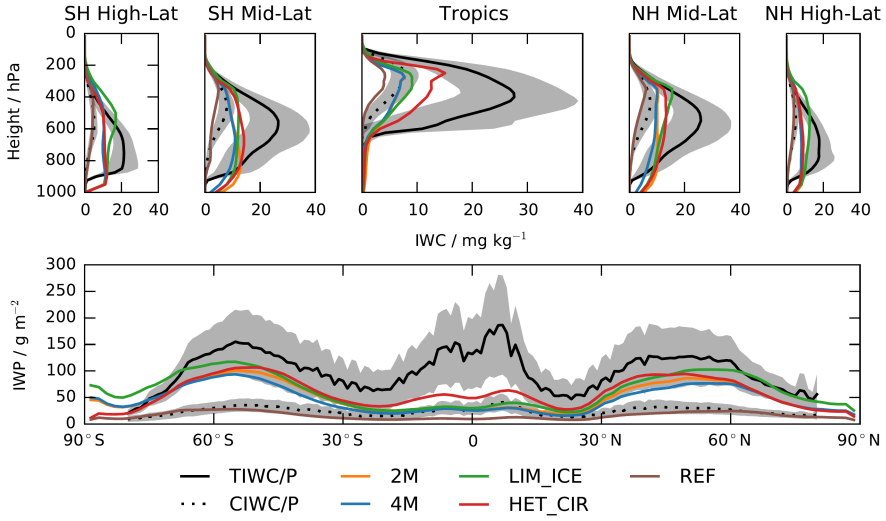

Figure 5. Ice water content and ice water path compiled from observations by Li et al. (2012) and different versions of ECHAM6-HAM2 (10 year, zonal averages) with the new microphysics scheme and the reference model. The top row shows vertical profiles for ice water content, the panel on the bottom shows ice water path. The observations in black include total ice water content/path (TIWC/P; solid lines) and cloud ice water content/path (CIWC/P; dotted lines). Colors show total (stratiform) ice water content from the new model and cloud ice water content from the reference model. The grey shaded areas represent the average standard deviation as reported by Li et al. (2012). The profiles are averaged over different latitude bands: SH High-Lat (80°S to 60°), SH Mid-Lat (60°S to 30°S), Tropics (30°S to 30°N), NH Mid-Lat (30°N to 60°N) and NH High-Lat (60°N to 80°N).

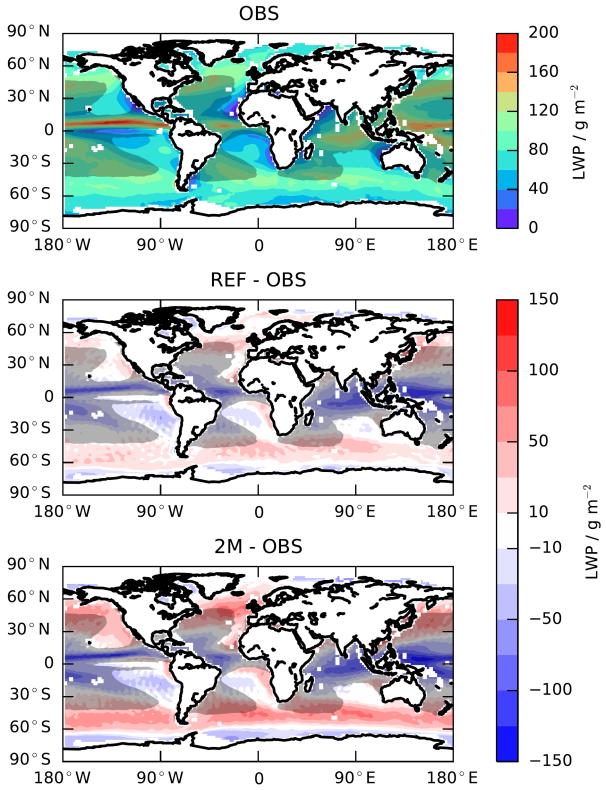

Figure 6. LWP as observed by the Multisensor Advanced Climatology of LWP (MAC-LWP), climatology from 2003 to 2012. The top panel shows the observations, the middle shows the difference between the new model (2M) and the observations and the bottom panel shows the difference between the reference model and the observations. The models are both run for 10 years from 2003 to 2012. The grey shaded areas show regions where the liquid water path is dominated by precipitation ($LWP/TWP < 0.8$), i.e. where there is no reliable estimate for in-cloud liquid water path.

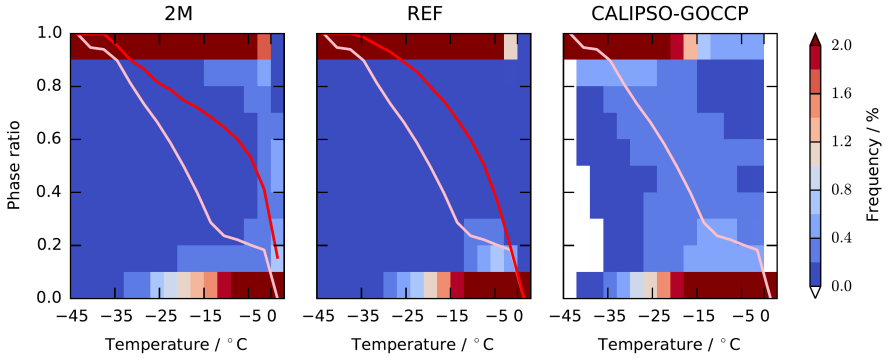

Figure 7. Frequency of cloud occurrence per temperature and phase ratio for histogram bin widths of 3 °C and 0.1, respectively. The average ice fraction per temperature bin is shown by the red line for the new model (2M; left) and the reference model (REF; middle). The pink line appears in every subplot and shows the ice fraction from the CALIPSO-GOCCP product. Both the models and observations are accumulated over night only. The models contain data from 10 years of simulation from 2003 to 2012. The satellite data is accumulated over 7 years from 2007 to 2013.

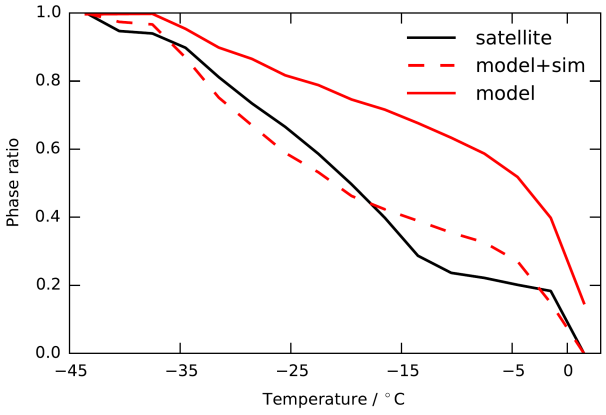

Figure 8. Frequency of cloud occurrence per temperature for histogram bin widths of 3 °C. The average ice fraction per temperature bin is shown for the model data (red, solid line), the CALIPSO-GOCCP product (black, solid line) and the output from the COSP simulator applied to the model (red, dashed line). The model and online simulator are run for one year.

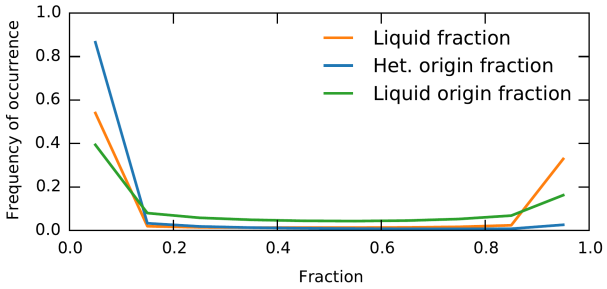

Figure 9. Frequency of cloud occurrence per ice source fraction for the liquid origin fraction F_{liq} and the different ice source fractions F_{het} and F_{liq-o}. The histogram bin width is 0.1. The lines are aligned with bin centers. Only gridboxes are sampled where all the fractions are well-defined, i.e. only cloudy gridboxes for F_{liq} and only gridboxes containing ice for F_{het} and F_{liq-o}. Data is sampled every time step for 10 years of simulation with the new model (2M).

Table 3. 10-year, global average values for a selection of key microphysical parameters for the model configurations presented in Table 2. Observational data is used from the compilation of Lohmann and Neubauer (2018) with the exception of ice water contents where we use the dataset of Li et al. (2012) and report their average standard deviation.

Simulation	OBS	2M	4M	LIM_ICE	HET_CIR	REF
LWP, g m^{-2}	81 (30 to 90)	73.5	76.6	73.4	64.2	64.9
TIWP, g m^{-2}	100±46	48.1	43.1	56.9	60.9	-
CIWP, g m^{-2}	24±10	-	-	-	-	14.8
N_c, 10^{10} m^{-2}	-	4.61	4.57	4.37	4.17	3.16
N_i, 10^{10} m^{-2}	-	0.10	0.10	0.14	0.04	0.08
CC, %	68±5	64.5	64.4	67.3	64.0	68.3
Q, kg m^{-2}	25.7	27.35	27.36	27.92	27.50	26.41
P_{tot}, mm d^{-1}	2.7±0.2	2.9	2.9	2.9	2.9	3.0
P_{strat}, mm d^{-1}	-	1.0	1.0	1.0	1.1	1.0
P_{cnv}, mm d^{-1}	-	1.9	1.9	1.9	1.8	2.0
SW CRE, W m^{-2}	-47.3 (-44 to -53.3)	-47.3	-47.3	-50.6	-47.2	-50.1
LW CRE, W m^{-2}	26.2 (22 to 33.5)	21.2	21.2	25.9	22.0	24.3
Net CRE, W m^{-2}	-21.1 (-17.1 to -22.8)	-26.1	-26.1	-24.7	-25.1	-25.8
TOA LW, W m^{-2}	-237 to -241	-238.5	-238.5	-234.2	-238.5	-237.8
TOA SW, W m^{-2}	238 to 244	239.4	239.4	236.2	239.1	238.1
Δ TOA, W m^{-2}		0.9	0.9	2.0	0.6	0.3

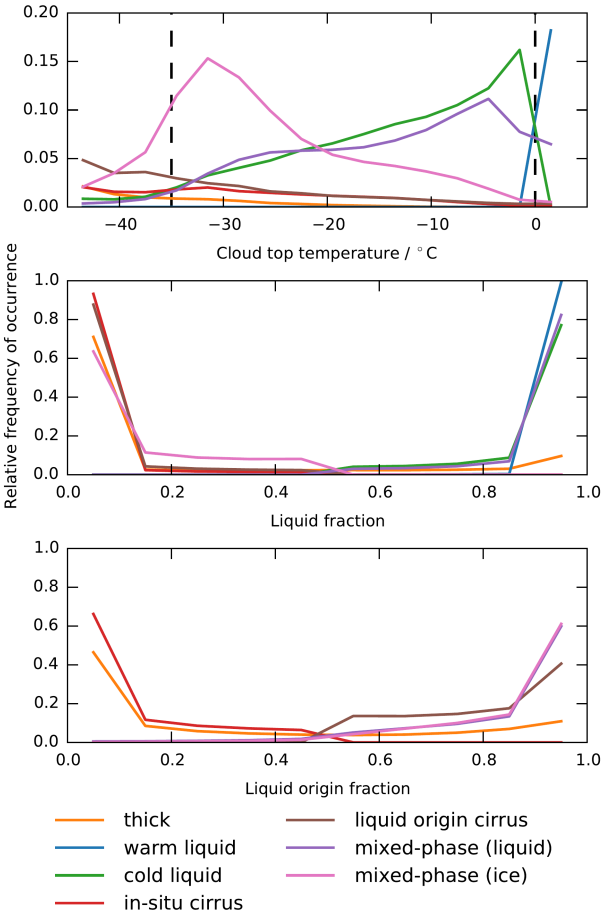

Figure 10. Relative frequency of cloud occurrence (normalized by the cloud type occurrence frequency). This corresponds to conditional probability histograms, $P(X_\bullet \in Bin|\boldsymbol{X} \in Type_i)$ for the model state $\boldsymbol{X}$ with components $X_\bullet$: cloud top temperature (top panel), liquid fraction (middle panel) and liquid origin fraction (bottom panel) for each cloud type i. Bin widths are $3\,^\circ\mathrm{C}$ for temperature and 0.1 for the dimensionless fractions respectively, lines are aligned with bin centers. Data is sampled every time step for 10 years of simulation with the new model (2M).

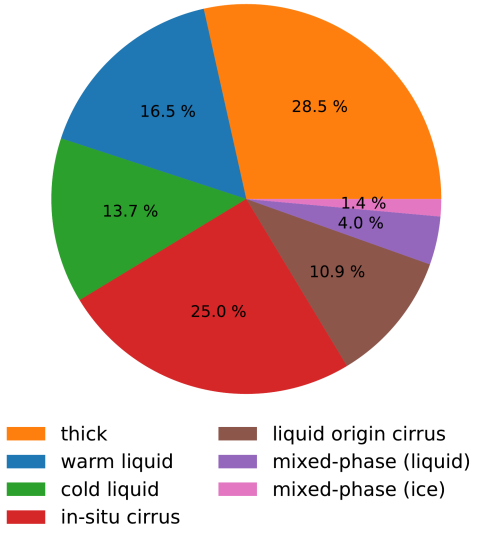

Figure 11. Global relative contribution to the 3D cloud volume (as measured by the air mass occupied) for the cloud types defined in Table 4 based on their formation pathways. Data is sampled every time step for 10 years of simulation with the new model (2M).

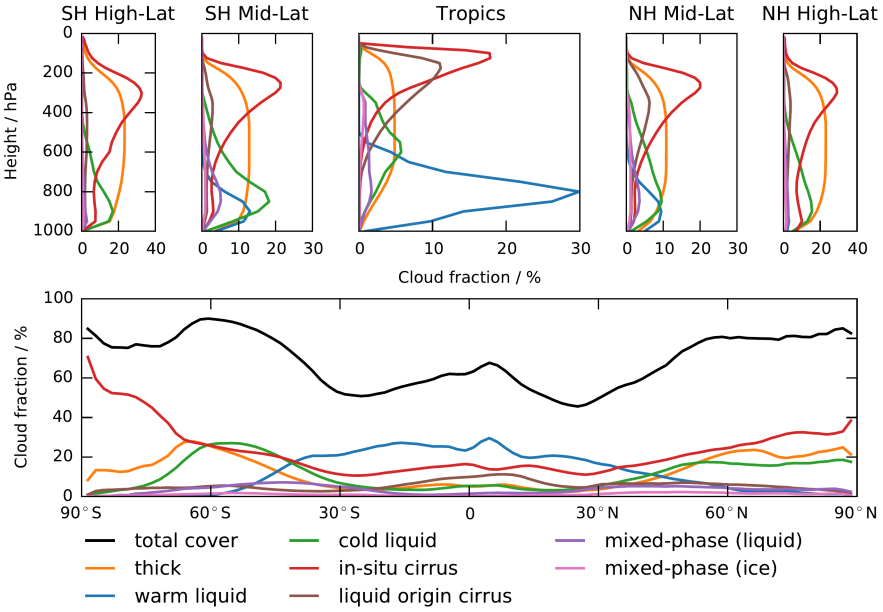

Figure 12. Same as in Fig. 5 but for the absolute frequency of occurrence profile (top panel) and relative contribution to the total cloud cover (bottom panel). The relative contribution is computed as the fraction of cloud volume occupied per column and cloud type. Data is sampled every time step for 10 years of simulation with the new model (2M).

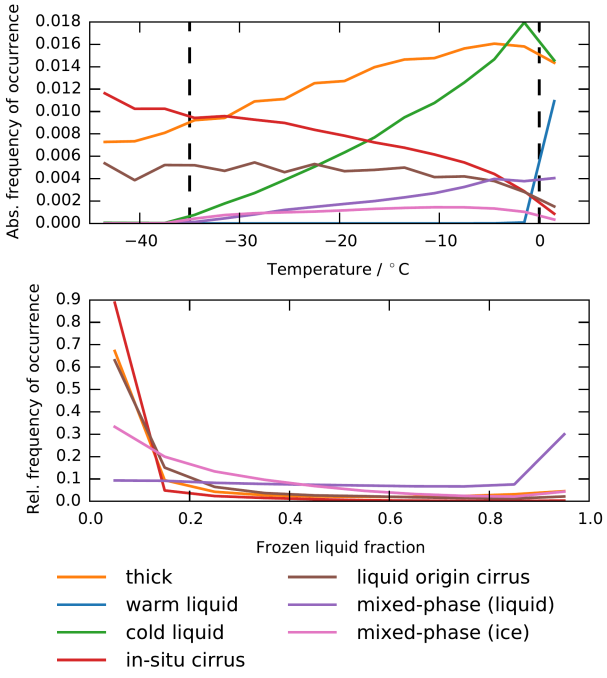

Figure 13. Frequency of occurrence for grid-box temperature (top) and frozen liquid fraction (bottom). For the temperature component X_T of the model state $\boldsymbol{X}$ we show the absolute frequency of occurrence $P(X_T \in Bin|\boldsymbol{X} \in Type_i) \cdot P(\boldsymbol{X} \in Type_i|X_b > 0)$. We only sample cloudy grid-boxes, i.e. those with a cloud fraction component $X_b > 0$. For the frozen liquid fraction component X_{Fliq-f} we show the relative frequency of occurrence $P(X_{Fliq-f} \in Bin|\boldsymbol{X} \in Type_i)$. The latter is the accumulated ice mass fraction that formed through any liquid water to ice conversion process (including the WBF process). Note that this is not equal to the liquid origin mass that quantifies the origin of cloud ice. Bin widths are $3\,^{\circ}\mathrm{C}$ and 0.1 respectively, lines are aligned with bin centers. Data is sampled every time step for 10 years of simulation with the new model (2M).

Table 4. Definition of cloud types. We categorize and separate clouds by exceeding thresholds of the 5 predictors: The heterogeneous freezing origin fraction F_{het}, cloud top to bottom pressure difference Δp, cloud liquid fraction F_{liq}, liquid-origin fraction F_{liq-o} and the cloud top temperature T_{top}. If a predictor is not used for a certain class, it is symbolized by a '$-$' sign.

Label	F_{het}	Δp	F_{liq}	F_{liq-o}	T_{top}
Thick clouds, homogeneous origin	< 0.5	$> 500\,\mathrm{hPa}$	$-$	$-$	$-$
warm liquid clouds	< 0.5	$< 500\,\mathrm{hPa}$	> 0.5	$-$	$> 0\,^{\circ}\mathrm{C}$
cold liquid clouds	< 0.5	$< 500\,\mathrm{hPa}$	> 0.5	$-$	$< 0\,^{\circ}\mathrm{C}$
Cirrus clouds, in situ	< 0.5	$< 500\,\mathrm{hPa}$	< 0.5	< 0.5	$-$
Cirrus clouds, liquid origin	< 0.5	$< 500\,\mathrm{hPa}$	< 0.5	> 0.5	$-$
Mixed-phase, liquid dominated	> 0.5	$-$	> 0.5	$-$	$-$
Mixed-phase, ice dominated	> 0.5	$-$	< 0.5	$-$	$-$